



Argelander-
Institut
für
Astronomie



Non-Accreting Helium Stars as Progenitors of Thermonuclear Supernovae

Masterarbeit zur Erlangung des akademischen Grades

Master of Science (M.Sc.)

im Studiengang Astrophysik

Angefertigt von

Savvas Chanlaridis

am

Argelander-Institut für Astronomie

Vorgelegt der

Mathematisch-Naturwissenschaftlichen Fakultät
der
Rheinische Friedrich-Wilhelms-Universität Bonn
Deutschland

October, 2019

I hereby declare that this thesis was formulated by myself and that no sources or tools other than those cited were used.

Date

Signature

1. Gutachter: Prof. Dr. Norbert Langer
2. Gutachter: Prof. Dr. Michael Kramer

τί δὴ τοῦτο ἐστι Πυθαγόρας ἐρωτώμενος,
τὸ θεάσασθαι εἶπε τὸν οὐρανόν

*When Pythagoras was asked [about the purpose
for which humans were created], he said,
“To look upon the heavens”*

ABSTRACT

Thermonuclear explosions of carbon-oxygen white dwarfs are being observed as Type Ia supernovae. Although the scientific consensus is that these transients originate in binaries, their progenitors as well as the associated explosion mechanism are much debated.

SNe Ia exhibit significant diversity in terms of their spectra and light curves, and thus, it is rather unclear if the companion star to the white dwarf is a non-degenerate star (single degenerate scenario), or another white dwarf (double degenerate scenario). In addition, there may be significant contributions from alternative channels.

In this thesis, we performed detailed numerical calculations with the MESA stellar evolution code in order to examine models of single, non-rotating helium stars as potential progenitors of SNe Ia. By adopting various initial values for the metallicity, and by allowing efficient overshooting mixing across convective boundaries, we found that the vast majority of He-stars in the initial mass range $1.9 - 2.7 M_{\odot}$ develop a degenerate ONe core, that retains a small amount of carbon. Subsequent shell burning can increase the mass of the core to the Chandrasekhar mass limit and ignite the residual carbon, resulting in a thermonuclear explosion.

In some limiting cases, the carbon-burning front that was created after helium depletion in the core, is stalled before it reaches the centre. This is caused by mixing that reduces the efficiency of carbon-burning, resulting in a hybrid-like structure where the inner CO core is surrounded by a processed ONe mantle. We found that even in this case, if the core of the hybrid star reaches the Chandrasekhar mass limit, compressional heating will ignite the carbon-rich core in a similar fashion to typical SNe Ia progenitors.

By performing a first-order estimation of the birth rate of these systems, we argue that in the absence of an extended accretion phase, these models can provide an alternative channel for SNe Ia progenitor systems with a non-negligible effect on the observed rate of SNe Ia.

ACKNOWLEDGMENTS

During my effort for the completion of this Master Thesis many people have stand by me and contributed in one way or another. First and foremost, I would like to thank my supervisor Prof. Dr. Norbert Langer for accepting me as a member of his group, his guidance, and for always being there when he was needed. His teachings, encouragement, and trust during the last year were all invaluable and something that I will always hold dear.

It is difficult to express my gratitude towards my advisor, Dr. John Antoniadis, in just a few lines. Thank you for the leap of faith you took, by taking me under your wings as an inexperienced graduate student with no degree of intuition for the field whatsoever. Hopefully my mistakes, and constantly naive questions have not left a permanent mark on your tolerance levels.

I am eternally grateful to Priv.-Doz. Dr. Jürgen Kerp for his trust and support by giving me the chance to improve my knowledge on radio-astronomical observations, and my communication skills as a teaching assistant. Our exciting conversations on topics not directly related to our work, opened my eyes to new perspectives.

I want, also, to thank Prof. Dr. Michael Kramer for agreeing to be my thesis evaluator on such a short notice, Dr. Götz Gräfener for illuminating discussions on stellar winds, and David Ramon Aguilera Dena for sharing with me pieces of his code.

There are no words to express my thankfulness to my family. Without their support, nothing would be possible to begin with. I cannot but devote this thesis to them.

To my girlfriend Anastasia for putting up with my frequent meltdowns, for her understanding, and for being abroad and not with her all of those years, I give my love.

Finally, to Tilemachos, Thaleia, Kostas, Eftychia, Miltos, Christos, and Despoina thank you for making my everyday life more tolerable and fun.

CONTENTS

Abstract	vii
Acknowledgments	ix
Contents	xi
List of Figures	xiii
List of Tables	xv
1 Introduction	1
1.1 Helium stars	1
1.1.1 Formation of helium stars	2
1.1.2 Evolution of single helium stars	2
Mixing mechanisms	4
Effects of rotation	5
Stellar winds and mass loss	6
1.2 Evolution of binary systems	6
1.2.1 Interaction and orbital parameters	6
1.2.2 Mass transfer	8
1.2.3 Common envelope	9
1.2.4 Angular momentum losses	9
1.2.5 Double neutron star systems	9
1.3 Stellar transients	11
1.3.1 Explosion Mechanisms	11
Iron core collapse SNe (Fe-CCSNe)	12
Electron capture SNe (ECSNe)	12
Pair instability SNe (PISNe)	13
1.3.2 Type Ia Supernovae	13
1.3.3 Type Ib/c Supernovae	13
1.4 Thesis Outline	14
2 Methods	15
2.1 Modules for Experiments in Stellar Astrophysics	15
2.1.1 Microphysics	16
Nuclear networks & reactions rate	16
2.1.2 Macrophysics	16
Mass loss	17

The mixing length theory	17
Thermohaline & Semiconvection	18
3 Type-Ia Supernovae from non-accreting progenitors	19
3.1 Introduction	20
3.2 (C)NeO cores: formation and evolution	20
3.2.1 Numerical Calculations: Input Physics	21
3.2.2 Simulation results	22
3.2.3 Late evolution and thermonuclear runaway	23
3.2.4 Energetics and nucleosynthesis	24
3.3 Expected rates and delay times	24
3.4 Summary	27
4 Helium Stars as Progenitors of Thermonuclear Supernovae	29
4.1 Introduction	30
4.1.1 Thermonuclear Supernovae	30
4.1.2 The Urca process	31
4.2 Stellar Evolution Code and Initial Parameter Space	32
4.2.1 Physical assumptions	32
4.3 Results	33
4.3.1 Overview of the Evolution	33
4.3.2 Core Growth and Structure	34
4.3.3 Wind and Envelope Ejection	35
4.3.4 The Role of Residual Carbon Oxygen-Neon Cores	36
Hybrid COnMg Cores	39
4.4 Discussion and Future Work	39
5 Conclusions and Outlook	43
Bibliography	52

LIST OF FIGURES

1.1	Evolution of the core as a function of central temperature (y-axis), and central density (x-axis). The point where the star enters the He-MS as a He-ZAMS can be seen as a small hook inside the black circle. An analytic explanation of the letters along the evolutionary tracks, is provided in the text. The coloured areas illustrate the different regimes of pressure.	3
1.2	Kippenhahn diagramm for a $3.0 M_{\odot}$ He-star with mass loss. The x-axis expresses the remaining time of the calculations, whilst the y-axis shows the inner structure of the star in terms of mass coordinates. The green and gold hatched areas denote convective and thermohaline mixing respectively. Red solid lines represent areas with semi-convective mixing. The black, red, and green dotted lines show the build-up of helium, carbon, and oxygen core mass respectively.	4
1.3	Left panel: Equipotential lines in the orbital plane of a rotating binary system, with a reduced mass ratio of $\mu = 0.316$. In this setup, M_1 is the more massive and is located at $x = +a$, whilst M_2 is the less massive and is at $x = -b$. The inner equipotential surface that passes from the L_1 Lagrangian point, defines the “teardrop”-shaped Roche-lobes, one for each star. Contour lines passing through the Lagrange points are marked with blue colour. The image was created based on a <code>python</code> script, courtesy of Zingale (2016). Right Panel: 3D representation of equipotential surfaces. The image was adapted from van der Sluijs (2006).	7
1.4	Illustration of the overall evolution of a binary system that leads to the formation of a double neutron star system. The resulted binary system merges within a Hubble time and produces a single black hole. Image and caption taken from Tauris et al. (2017).	10
1.5	Basic classification of supernovae based on spectroscopic features. The absence of hydrogen lines in their spectra, distinguish type I from type II SNe. The presence of silicon, or helium absorption lines, create several subclasses within type I. In any case, further sub-groups can be identified if we take into consideration the behaviour of their light curves.	11
3.1	Kippenhahn diagrams following the evolution of $M_1 = 2.5 M_{\odot}$ (left) and $M_2 = 1.8 M_{\odot}$ He-stars, after core helium depletion. The x-axis represents star’s age, whilst the y-axis shows the inner structure of the star in terms of mass coordinate. Colored areas indicate regions in which nuclear burning occurs, i.e. locations for which the nuclear energy ϵ_{nuc} exceeds energy losses due to neutron emission, ϵ_{ν}	22
3.2	Evolution of the core density and temperature for M_1 and M_2 . The dashed line shows the approximate boundary for electron degeneracy. Burning thresholds for a 100% abundance of the corresponding species are indicated with dotted lines. The nuclear statistical equilibrium threshold assumes an equilibrium timescale of 1 s.	24

3.3	Density profiles at maximum compactness (solid lines) and at the end of our MESA calculations (dashed lines). M1 and M2 refer to He-stars with initial mass $2.5 M_{\odot}$ and $1.8 M_{\odot}$ respectively. Regions indicating approximate burning regimes as in Seitenzahl & Townsley (2017).	25
3.4	Overview of the different systems contributing to the SN Ia channel discussed in the text, on the mass-mass plane. Hatched regions represent initial mass-range for which a thermonuclear explosion may occur. Binary systems outside those mass-ranges can enter the hatched regions via binary interactions, as indicated by the arrows.	26
4.1	Kippenhahn diagram of the $2.5 M_{\odot}$ helium star with $Z = 0.02$ and no overshooting that leads to the final structure shown in Fig. 4.6c. The x-axis is expressed in terms of model number, whilst the y-axis shows the inner structure of the star in terms of mass coordinate. Blue areas denote regions with convection; green-coloured areas indicate thermohaline mixing. The intensity shown in the colour-bar, indicates the net energy-production rate. During electron captures on ^{24}Mg and subsequent carbon burning, the core becomes convective.	35
4.2	Full parameter space of our considered stellar model grid. Metallicity for the bottom, middle, and top panel is $Z = 0.0001$, $Z = 0.001$, and $Z = 0.02$ respectively, whilst the color-bar indicates the composition of the model at the moment our simulation was terminated. Red pixels represent models that have developed a silicon core and will evolve towards a core collapse supernova (CCSN). Hatched regions show models that have developed a core mass in the range $1.35 - 1.37 M_{\odot}$, and can experience a thermonuclear runaway (see text for caveat).	36
4.3	Final core mass of our models as a function of initial mass, for various initial metallicities (left) and overshooting factors (right). Models that experience thermal runaway develop a core of $M_c \sim 1.36 \pm 0.01 M_{\odot}$ (plateau) due to He-shell burning. Missing data points correspond to models which their evolution ended abruptly, hence their final core mass could not be estimated.	37
4.4	HertzsprungRussell diagram expressed in terms of luminosity (y-axis) and effective temperature (x-axis), for our $2.5 M_{\odot}$ fiducial model, starting from helium main sequence phase. During the shell-burning phase, the star reach extremely high, super-Eddington luminosities (up to $\log L/L_{\odot} = 6.25$) that strips its envelope away.	37
4.5	Examples of the evolution of different initial masses in the $\log(\rho_c) - \log(T_c)$ plane. Black dotted lines show approximate ignition curves taken from MESA. Black dashed lines indicate different pressure regimes whilst the red dashed curve shows the approximate threshold for e-captures on ^{20}Ne nuclei. The blue dashed line refers to the same stellar model as the one with the solid blue line; the only difference is that for the former, all carbon-participating reaction have been switched off leading most likely to an ECSN.	38
4.6	Abundance profiles of our fiducial models during various evolutionary stages. Panels (a) and (b) refer to the abundance profiles when $\log(\rho_c/\text{gr cm}^{-3}) \approx 9.0$ (indicated by the grey circle in Fig. 4.5). In panel (d), the core reaches the density threshold for e-captures on Ne nuclei to commence, leading to formation of ^{20}O , and most likely to an ECSN.	40

LIST OF TABLES

4.1	Baseline parameters for single helium stars	33
4.2	Stellar parameters for twenty-two single helium stars, evolved to the pre-SN stage. Models that were able to evolve after oxygen ignition are indicated with an asterisk in the comments. X_9 refers to the core mass fraction when $\log(\rho_c/\text{gr cm}^{-3}) \approx 9.0$. As ignition density we consider the maximum density before the thermal runaway.	41

Chapter 1

INTRODUCTION

The cycle of life and death of stars baffled astronomers for many years. The study of stellar structure and evolution continues—up to this date—to be of paramount importance, since it is crucial to our understanding of various branches of astronomy, e.g. the structure of galaxies, and chemical history of the Universe.

The aim of this thesis is to provide new insights into one of the most debated topics in Stellar Astrophysics: the connection between type-Ia supernovae and their progenitor systems. The observed diversity among SNe-Ia spectra indicates that there may be more than one formation channels, and although all existing models are promising, one needs to investigate alternative paths (e.g. [Nomoto et al. 1997](#); [Iben 1997](#); [Langer et al. 2000](#); [Hillebrandt & Niemeyer 2000](#)).

The lack of a hydrogen mantle makes helium stars a natural choice as potential candidates of supernovae of type I, since hydrogen absorption lines are absent from the early spectra of the latter. In this chapter, a synopsis that extends from the formation to the death of these stars will be attempted. Our intention is not to provide a detailed coverage of the principles of stellar evolution, but rather a small introduction to several fundamental notions, tailored to our needs. More technical details follow at the begining of each chapter. Nevertheless, for the interested reader that finds this chapter difficult to follow, there are classical textbooks ([Kippenhahn et al. 2012](#); [Clayton 1968](#); [Prialnik 2000](#); [Eggleton 2006](#)) which cover almost every aspect of the field of stellar astrophysics.

1.1 Helium stars

From the large primordial molecular clouds, stars are being constantly formed as a result of turbulent motions that cause parts of them to collapse under their own gravitational attraction ([Klessen 2011](#); [Jappsen, A.-K. & Klessen, R. S. 2004](#)). When the accretion of the surrounding material from the protostellar core ceases, the protostar is said to be in the *pre-main sequence* (PMS) phase of its evolution, and continues to contract under the force of gravity until the central temperature becomes sufficiently high for nuclear fusion reactions on hydrogen to occur. At this point, the star enters the *main sequence* (MS) evolutionary phase as a zero-age main sequence (ZAMS) star where it will spend most of its life.

During the MS stage, the star converts hydrogen to helium either via the pp-chain reactions, or via the CNO cycles, depending on its initial mass and chemical composition. Slowly but steadily, the hydrogen in the core is being consumed by the aforementioned burning processes, and helium builds up forming a helium core. This process continues until the hydrogen in the stellar core is depleted, resulting in an inert hydrogen envelope engulfing the newly formed He-core; subsequently, the star exits the MS phase and the nuclear reactions in its interior that provided the necessary pressure support against gravity, effectively stop. Since the star is not in an equilibrium state anymore, it starts to contract until hydrogen

is ignited in a shell around the inert helium core. At this point, the star enters the so-called *red-giant branch* (RGB) and the hydrogen-rich envelope, on top of the H-burning shell, inflates rapidly whilst the He-core continues to contract due to the *mirror principle* (see Kippenhahn et al. 2012, p. 369).

As explained below, the hydrogen envelope can be lost when the star is in the RGB phase, with more than one ways, exposing the He-core of the star. This naked, hydrogen deficient He-core is what we refer to as a *helium star*. We can classify He-stars into two groups: low-mass *hot subdwarfs* (sd) that can be further subdivided into several categories (e.g. sdB, sdO) based on their spectra, and more massive *Wolf-Rayet* (WR) stars that can also be subdivided into several classes (e.g. WN, WC). For a more detailed discussion we refer the reader to the work of Han et al. (2002); Han et al. (2003); Heber (2009); Chiosi & Maeder (1986); Langer (2012).

1.1.1 Formation of helium stars

Helium stars can be formed either in isolation or in a multiple system. In either scenario, the physical mechanism responsible for the stripping of the hydrogen envelope is of the utmost importance.

In the former case of a single He-star, the necessary mass loss is being achieved due to strong, radiation-driven, stellar winds. However, the specifics of such a process have not been fully resolved yet, and an enhanced mass loss scheme, e.g. caused by rotational mixing, magnetic fields, or even strong He-flashes could result in the formation of the He-star (Sweigart 1997; Heber 2009).

In the case where the He-star progenitor is part of a binary system, the required strong mass loss can be achieved via different channels, depending on how wide the binary system is. These channels include the stable Roche-lobe overflow (RLO) and the Common Envelope (CE) ejection. We will discuss these mass loss mechanisms below. It should be mentioned that sdB stars can also originate from the merging of two helium white dwarfs (He-WD) in a close binary, resulting to an object with enough mass to ignite helium (Han et al. 2002).

1.1.2 Evolution of single helium stars

Once the He-star has formed, the compression of its core continues until it reaches the necessary conditions for helium to ignite at its centre. The ignition of core helium burning signifies the transition to the helium main sequence (He-MS) as a He-ZAMS star. The last two concepts are defined in a similar way to the (hydrogen) main sequence and ZAMS respectively.

During the He-MS stage, the star burns its ^4He supply via the triple-alpha process producing carbon (^{12}C) and oxygen (^{16}O). When the helium in the core is depleted, the contraction/expansion process we described above is repeated; the core now consists mainly of alpha elements and is surrounded by a He-rich envelope. This whole structure will contract until helium is ignited in a shell at the bottom of the envelope, followed by the ignition of carbon in the centre (given that the star is massive enough). The fate of the He-star at this point depends on its mass; if it has not retain enough mass for carbon ignition, it will gradually cool off and end its life as a carbon-oxygen white dwarf (CO WD). On the other hand, if it is massive enough to ignite carbon, either on or off centre, its fate could be an oxygen-neon-magnesium white dwarf (ONeMg WD), a hybrid white dwarf (CONeMg WD), or even collapse as a supernova (see Denissenkov et al. 2013; Chen et al. 2014).

To demonstrate the aforementioned stages, the evolutionary track of a 3.0 M_\odot He-star (with and without mass loss) is illustrated in the $T_c - \rho_c$ plane (Fig 1.1) (see also Habets 1986a,b; Nomoto 1987). The letters denote the beginning and end of several phases up to the off-centre neon ignition. The A-B phase shows the contraction that follows after the RGB stage of the progenitor. The moment of core He-ignition is denoted by the black circle at point B, and marks the entrance to the He-MS phase (B-C). At point C, helium has been exhausted and the core contracts whilst He-shell burning follows. During the D-E phase, the carbon is ignited in the core making a loop in the diagram around $\rho_c = 10^6 \text{ g cm}^{-3}$.

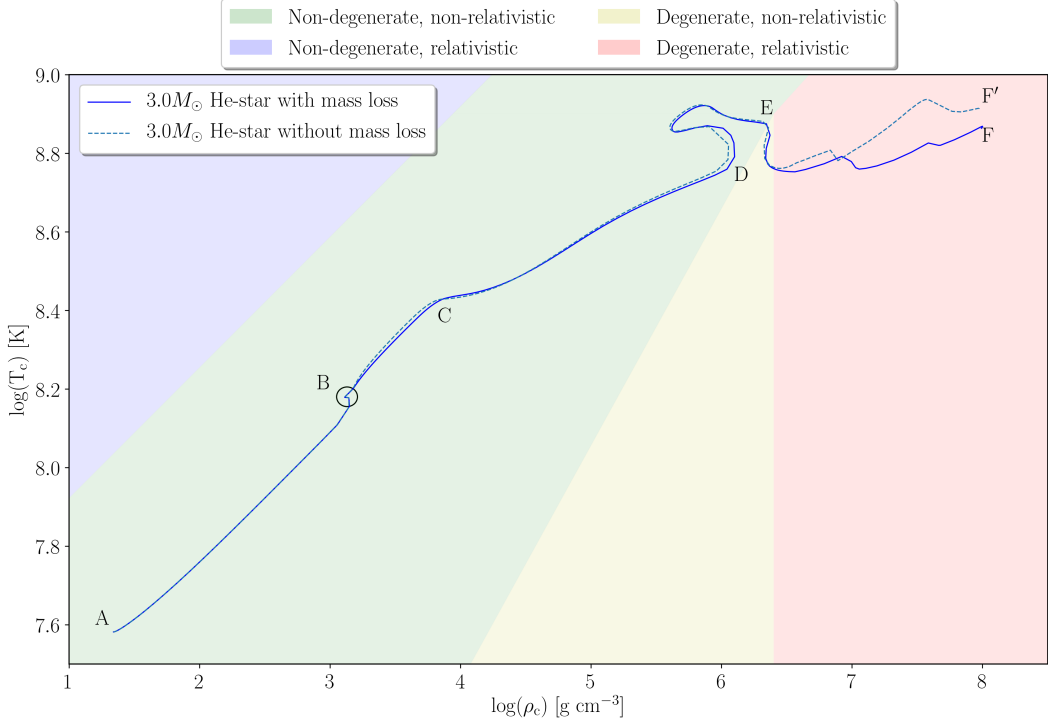


Figure 1.1: Evolution of the core as a function of central temperature (y-axis), and central density (x-axis). The point where the star enters the He-MS as a He-ZAMS can be seen as a small hook inside the black circle. An analytic explanation of the letters along the evolutionary tracks, is provided in the text. The coloured areas illustrate the different regimes of pressure.

Finally, the E-F/F' shows the carbon-shell burning along the contraction of the ONeMg core; at the endpoint (F/F'), neon is ignited off-centre.

Conveniently, in the same figure one can see the approximate regimes of pressure which are illustrated as coloured regions. For the conditions in the green area, the stellar material is non-degenerate and non-relativistic hence the dominant pressure can be approximated by the ideal gas law (P_{gas}). The blue area shows the region where the gas is still in a non-degenerate state but the temperature is so high that forces the electrons to move with speeds that are comparable to the speed of light. Under these conditions, the pressure provided by the exerted radiation (P_{rad}) begins to dominate over the gas pressure. Moving to higher densities the electron gas becomes degenerate, first non-relativistically (yellow area) and then relativistically (red area). In both cases the pressure is provided by the degenerate electron gas, although the degeneracy can be lifted if the temperature is sufficiently high.

These boundaries for the pressure regimes can be easily found if one equates the relevant expressions of pressure given by the equation of state for each regime (e.g. $P_{\text{gas}} = P_{\text{rad}}$, for the two non-degenerate regions). In reality, the transition among the different regimes is continuous and not sharp as depicted here, which can be misleading. Nevertheless, this simplified picture provides us with a visual aid of when in the evolutionary stage of a star relativistic, or quantum mechanical effects can be of great importance.

For a more complete and comprehensive overview of the evolution of single He-stars, we provide, in the form of a Kippenhahn diagram, the net energy production rate with respect to the internal structure of the $3.0 M_{\odot}$ star (with mass loss) we used in the example above (Fig 1.2). In this diagram, the x-axis expresses the remaining time of the calculations whilst the y-axis shows the inner structure of the star in terms of mass coordinates. The color scale is associated with the energy production. One sees that during He-burning in the convective core, the star experiences an approximately $\sim 0.3 M_{\odot}$ mass loss via stellar winds. As a result of this core burning process, a C-core of $\sim 1.2 M_{\odot}$ is formed that continues to

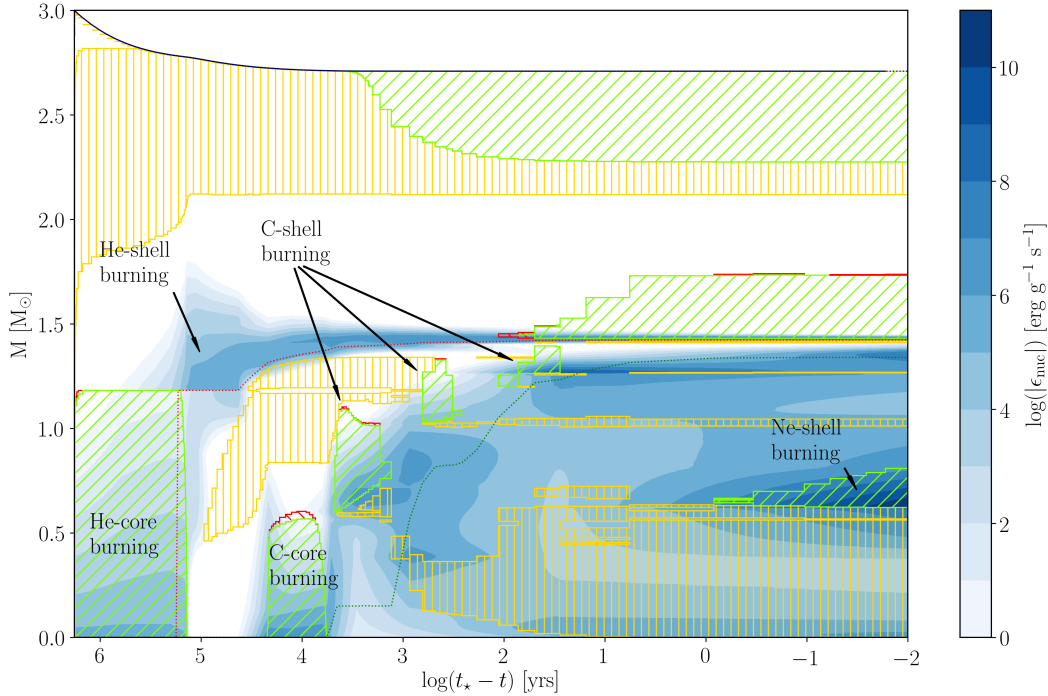


Figure 1.2: Kippenhahn diagramm for a $3.0 M_{\odot}$ He-star with mass loss. The x-axis expresses the remaining time of the calculations, whilst the y-axis shows the inner structure of the star in terms of mass coordinates. The green and gold hatched areas denote convective and thermohaline mixing respectively. Red solid lines represent areas with semi-convective mixing. The black, red, and green dotted lines show the build-up of helium, carbon, and oxygen core mass respectively.

grow up to $\sim 1.42 M_{\odot}$ due to He-shell burning. Similarly, an oxygen core is formed as a result of the more advanced burning stages.

Mixing mechanisms

Although protostars begin their life with, a more or less, uniform elemental composition which is the same as the composition of the cloud they originated from, the ongoing nuclear reactions transform and create new elements that are not necessarily distributed uniformly throughout the stellar interior. These mixing mechanisms are usually caused by various instabilities and can contribute at different levels based on specific conditions. In this section we will briefly explain four major mixing processes leaving the effects of rotation for later discussion.

The most effective way to transfer material is with *convection*. Thermal variations across different shells of the star will lead to density variations and, consequently, to buoyancy driven flows of the fluid. Essentially, what this means is that a hot parcel of fluid will rise due to buoyancy forces and a colder parcel will sink. This process is very efficient for transporting more heavy elements produced in the deep interior of the star towards the surface via bulk motions (dredge-up) and vice versa. The stability of a layer against convection is given by the *Ledoux* criterion

$$\nabla_{\text{rad}} < \nabla_{\text{ad}} - \frac{\phi}{\delta} \nabla_{\mu} \quad (1.1)$$

which, in the case of chemically homogeneous layers ($\nabla_{\mu} = 0$), reduces to the *Schwarzschild* criterion

$$\nabla_{\text{rad}} < \nabla_{\text{ad}} \quad (1.2)$$

where ∇_{rad} is the radiative temperature gradient describing the logarithmic temperature variation with depth (for the case that energy is transported by radiation); ∇_{ad} is the adiabatic temperature gradient defined similarly to ∇_{rad} but for the case of adiabatic compression or expansion; and the second term of the equation accounts for changes in chemical composition. For a detailed explanation of the symbols and the implications of those criteria, see (Kippenhahn et al. 2012, pp. 49-51).

The composition gradient in the Ledoux criterion acts as a stabilizing agent in weakly, thermally unstable regions leading to a slower mixing rate. These zones are not mixed by convection but rather by another process, called *semi-convection* (see also Section 2.1.2, and Spruit 2013; Langer et al. 1983; Langer 1991).

Another mechanism that has an important consequence in stellar evolution, is *convective overshooting*. During this phenomenon, a parcel of fluid carried away by convection will overshoot beyond the boundary of the unstable region and into the stable region. This is caused by the inertia of the convective material and thus, it travels some distance further than the region in which it was accelerated until it loses all of its momentum. For this reason, convective overshooting introduces a large uncertainty in the extent of mixed regions (see Saslaw & Schwarzschild 1965; Stothers & Chin 1990; Roxburgh 1998, for a detailed discussion on the effects of overshooting).

The fourth major mixing process is called *thermohaline* mixing. It occurs when the molecular weight decreases with depth, e.g. a helium layer on top of a hydrogen-rich layer due to accretion in a binary system. The heavier elements will eventually sink in whilst the lighter material will rise, re-establishing the mean molecular weight to being larger as we move towards the centre of the star¹. However, thermohaline mixing is believed to play a lesser role in the evolution of single stars and becomes important in accreting binaries (see also Cantiello, M. & Langer, N. 2010; Charbonnel, C. & Zahn, J.P. 2007).

Effects of rotation

The evolution of stars can be significantly altered if they are rotating. This is true for most—if not all—stars found in nature, since they inherit angular momentum during the collapse of the already turbulent molecular cloud they originated from. Rotation can influence the shape of stars, their lifetimes since the centrifugal force lowers the internal pressure that is necessary to balance gravity, and their abundance profiles. The latter is a result of several rotation-induced instabilities like the Eddington-Sweet circulation, the dynamical shear instability, and the secular shear instability, to name a few. Especially the Eddington-Sweet circulation and the shear instability play an important role to the transportation of angular momentum between different layers of the star.

The importance of rotational mixing is difficult to overstate. As an example, we mention the results of Maeder (1987) who found that, for massive stars, a bifurcation of the evolutionary tracks in the Hertzsprung-Russel diagram appears around a critical rotation. This is caused by the inability of the composition gradient (∇_{μ}) to prevent turbulent diffusion above this critical rotation, thus the diffusive mixing leads to an almost chemically homogeneous evolution, i.e. the star exhibits the same composition everywhere. These homogeneous models are likely to result to the formation of WR stars before the end of their hydrogen-burning phase, which increases the WR lifetime, and potentially lead to the formation of gamma-ray bursts in low-metallicity environments (Yoon & Langer 2005).

A detailed coverage of the effects of rotation in stellar evolution is offered by Langer et al. (1997); Heger et al. (2000); Hirschi et al. (2004); Maeder et al. (2006); Langer (2012); Palacios (2013). More on the rotation-driven transportation of angular momentum and associated mechanisms can be found in Heger et al. (2005); Langer (2012) as well as in the work of Spruit (2002) where a discussion on the importance of dynamo-generated magnetic fields takes place.

¹This is a slow process since gravitational settling can be balanced by a supporting temperature gradient that could lead to the formation of doubly diffusive instabilities (e.g. salt-fingers).

Stellar winds and mass loss

It has been long since we first discovered that stars experience a continuous outflow of material from their surface, causing them to gradually lose a significant fraction of their initial mass. This loss of material is called *stellar wind* and several mechanisms trying to explain its origin have been proposed over the years.

Stellar winds do not affect all stars in the same way, but they depend on the mass of the star and its current evolutionary stage. Low-mass stars that are in the MS phase, like our Sun, are hardly influenced from the generated winds. However, more massive and post-MS stars experience strong, usually radiation driven², winds that peel off large amounts of mass, and changing this way their surface chemical composition. The mass loss rates and the terminal velocities of these winds appear to vary significantly with luminosity, temperature, metallicity, and other global stellar parameters such as the radius (Hamann et al. 1982; de Jager et al. 1988; Nugis & Lamers 2000; Yoon 2017).

Observations of spectral features have allowed us to establish several empirical relations and constraints for the mass loss rates; especially in the case of WR stars which are known for their strong optically thick winds, the mass loss rates have been revised downwards by almost an order of magnitude (Nugis & Lamers 2000) compared to earlier estimations (Hamann et al. 1995; Langer 1989) due to the influence of clumping and the asymmetrical structure of the winds. The prescription of Nugis & Lamers (2000) is currently the most popular for the mass loss rate of WR stars (see also Section 2.1.2), although Yoon (2017) argues that in the aforementioned prescription, the considered metallicity dependence is not related to the initial metallicity, but rather to the self-enrichment of carbon and oxygen at the surface due to mass loss (see also Woosley 2019).

Finally, it should be mentioned that in the case of rotating stars, stellar winds will also carry away some of the specific angular momentum of the star along with the ejecta material. Additionally, magnetic fields coupled to the wind plasma in a co-rotation, will slow down the star which, in turn, will affect the mass-loss rate and the angular momentum losses of the system. This effect is known as *magnetic braking* and plays an important role in stellar evolution, especially in the case of binary systems (see Ivanova & Taam 2003). For a complete review of our current understanding of stellar winds see Lamers & Cassinelli (1999); Smith (2014).

1.2 Evolution of binary systems

So far we have outlined the evolution of single He-stars. However, the majority of stars are formed in multiple systems, that are gravitationally bound to each other. If the two stars are well separated, then the interaction between them should be minimal and both stars will evolve essentially as if they were isolated. In the case of a close binary, binary interactions might initiate mass transfer from one star to the other, altering significantly their structure, mass, angular momentum and, their final fate.

In the next few pages, we briefly explain the basic concepts that govern interacting binary systems. At the end, we will comment on the formation of double neutron star (DNS) binaries which is of particular interest for the aim of this thesis. For a more detailed coverage of the evolution of binary systems we refer to Ivanova (2015); Podsiadlowski (2014); Postnov & Yungelson (2014); Eggleton (2006); Tauris & van den Heuvel (2006).

1.2.1 Interaction and orbital parameters

In any multiple star system, the gravitational fields of all interacting components influence gravitationally the motion of the whole system. This is dubbed as *n-body problem* and is one of the most notoriously

²These winds can be driven either by radiation pressure on dust condensations that have been formed in the upper atmosphere of stars, or by radiaton pressure on the resonance absorption lines of metals such as carbon and nitrogen.

difficult problems in physics since it exhibits a chaotic behaviour with no general analytical solution; for this reason, a numerical approach is required.

In the case of a binary system, the n-body problem is reduced to the *restricted three-body problem* with the effective gravitational potential

$$\Phi = -G \left(\frac{M_1}{r_1} + \frac{M_2}{r_2} \right) - \frac{1}{2} \Omega^2 r_3^2 \quad (1.3)$$

where r_1, r_2 are the distances to the centre of the stars M_1 and M_2 respectively; Ω is the orbital angular velocity; and r_3 is the distance to the rotational axis of the binary (Tauris & van den Heuvel 2006, p. 639). If we require the cumulative forces acting on a test mass, m , to vanish

$$\mathbf{F}_t = -m\nabla\Phi = 0 \quad (1.4)$$

then Eq. 1.3 yields five stationary solutions where the gravitational force cancels out the centrifugal force caused by the relative motion of the two stars around each other. The points where Eq. 1.4 holds true, are called *Lagrangian points* or *libration points*, L_n , $n = 1, 2, 3, 4, 5$ (see Fig 1.3). Hence, if a test mass was to be positioned in any of those five equilibrium points, it would maintain its position relative to the two stars. More information on the stability of Lagrangian points, in the sense of what would happen if one applied a small perturbation on a test mass sitting in a libration point, can be found in Szebehely (1967); Celletti & Giorgilli (1990); Schwarz et al. (2012).

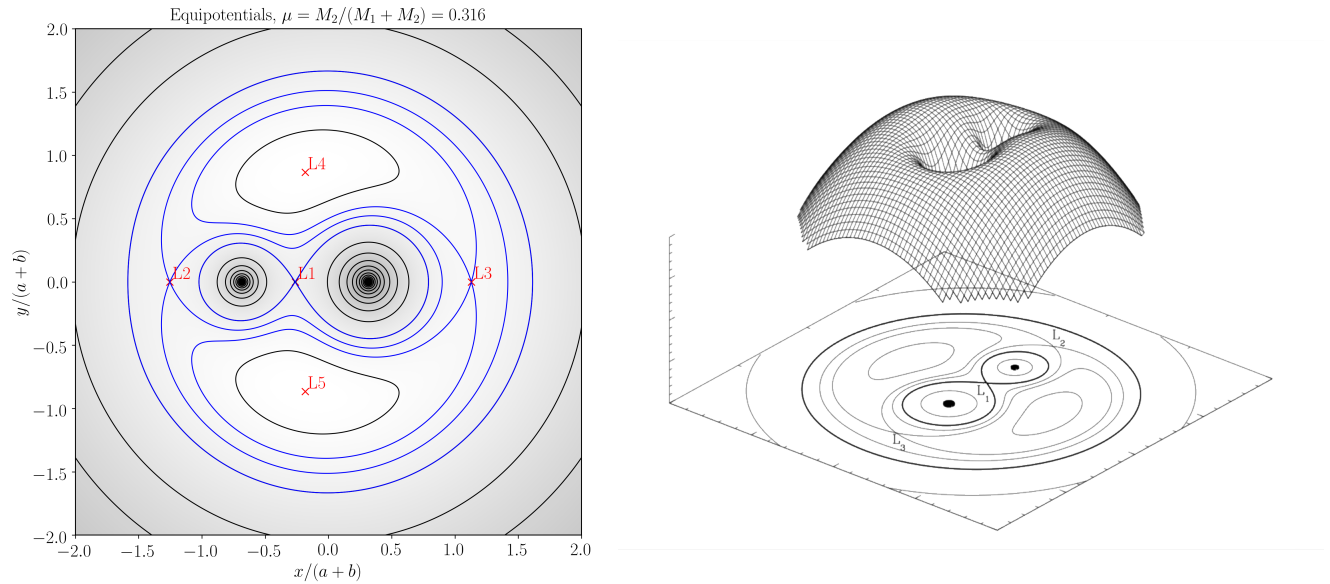


Figure 1.3: **Left panel:** Equipotential lines in the orbital plane of a rotating binary system, with a reduced mass ratio of $\mu = 0.316$. In this setup, M_1 is the more massive and is located at $x = +a$, whilst M_2 is the less massive and is at $x = -b$. The inner equipotential surface that passes from the L_1 Lagrangian point, defines the “teardrop”-shaped Roche-lobes, one for each star. Contour lines passing through the Lagrange points are marked with blue colour. The image was created based on a python script, courtesy of Zingale (2016). **Right Panel:** 3D representation of equipotential surfaces. The image was adapted from van der Sluijs (2006).

From the five Lagrangian points, L_1 plays a key role in the evolution of binary systems since the equipotential surface³ passing through that inner point, defines the *Roche-lobe*. The shape of the equipo-

³An equipotential surface is defined as the collection of all points in the system that share the same value of the effective gravitational potential, Φ .

tential surfaces is illustrated in Fig. 1.3; they assume a concentric spherical shape in proximity to the two stars whilst, as a result of the combined gravitational influence of the two masses, they get distorted when we move further away.

During the various evolutionary stages, the star might inflate and increase its radius to such a degree that the volume of the star exceeds the volume defined by its Roche-lobe. This will cause a transfer of surface material from that star to its companion via the L_1 point, triggered by the unbalanced pressure in that direction; this process is known as *Roche-lobe overflow* (RLOF) and the donor star can lose a substantial amount of its total mass. Unfortunately, there is no analytical expression for the size of the Roche-lobe in a given binary. However, [Eggleton \(1983\)](#) has proposed a numerical approximation of the radius of the Roche-lobe given by the following equation

$$\frac{R_L}{\alpha} = \frac{0.49q^{2/3}}{0.6q^{2/3} + \ln(1 + q^{1/3})} \quad (1.5)$$

where α is the orbital separation, and $q \equiv M_{\text{donor}}/M_{\text{accretor}}$ is the mass ratio of the binary components. These are the two most important orbital parameters that we need to know in order to follow the evolution of the binary.

It is worth mentioning that as matter spills across the inner Lagrangian point, it forms an *accretion disk* rather than falling directly onto the companion star. This happens because the accreted material possesses the same angular momentum as the donor star, and unless there are non-conservative processes able to remove some of the angular momentum of the accreted gas, it will continue to orbit around the companion star.

Depending on which equipotential surfaces are filled, one can classify binary systems into three categories (see also [Weigert 1968](#)): (i) *detached binaries* where the radii of both stars are smaller than their orbital separation; neither of the two stars fills its respective Roche-lobe, and they evolve almost independently of each other, (ii) *semi-detached binaries* where only one of the two stars fills its Roche-lobe leading to distortion of the equipotential surfaces from their spherical shape, and mass transfer occurs, and (iii) *contact binaries* where both stars fill their Roche-lobe. This situation results to a shared, common atmosphere that might be ejected, stripping the system from a significant amount of mass.

1.2.2 Mass transfer

From the discussion above, it becomes clear that the mass transfer rate via RLOF and its stability depends on the extent to which the donor star overfills its Roche-lobe. Especially the stability of the mass transfer depends on how the donor star responds to this sudden mass loss; for *stable* mass transfer, the donor must remain within its Roche-lobe (see [Ivanova 2015](#); [Postnov & Yungelson 2014](#); [Soberman et al. 1997](#); [Kalogera & Webbink 1996](#), for discussion).

Based on the evolutionary status of the donor star when it fills its Roche-lobe, we can discern three cases of mass transfer ([Kippenhahn & Weigert 1967](#); [Lauterborn 1970](#)):

- (i) *Case A*: mass transfer commences while the star is still in the MS, i.e. during core hydrogen burning;
- (ii) *Case B*: the donor star fills its Roche-lobe after the hydrogen has been depleted from its core but before helium ignition;
- (iii) *Case C*: refers to RLOF after the exhaustion of helium in the core, and includes all the subsequent stages.

For helium stars in particular, one can define the cases *BA*, *BB*, and *BC* for mass transfer during He core burning, He-shell burning, and carbon core burning respectively.

Finally, if the donor star is massive enough, it is likely to experience very strong stellar winds that will remove a considerable amount of mass even without RLOF. A fraction of this mass lost via winds might be accreted by the companion star; this is referred to as *wind mass transfer*, and although it provides a less efficient way to transfer mass, compared to RLOF, it can be important in some binaries.

1.2.3 Common envelope

When mass is transferred via RLOF in a dynamically unstable manner, i.e. when the convective envelope of the donor star continues to expand despite the mass loss, the mass loss rate naturally increases. The companion star accretes material stably at its thermal timescale, which is orders of magnitude larger than the dynamical timescale at which the donor star loses mass, thus it grows until it fills its Roche-lobe as well (Izzard et al. 2012); at this point, the two stars form a contact binary system, and share a common envelope (CE).

Since the orbital plane of the two stars lies within the CE, a drag force will be developed due to friction, caused by the motion of the stars. The system then goes through a *spiral-in* phase, during which a dissipation of orbital angular momentum leads to the decay of the orbit (i.e., a reduction of the orbital separation). This plunge phase occurs on dynamical timescale of a few years (Izzard et al. 2012), and the energy lost from the orbit is being deposited in the surrounding envelope. The reaction of the envelope to this energy deposition is to expand and potentially ejected from the binary. The ultimate outcome of the CE stage is either a more tight binary with a reduced total mass, or a merging event of the two cores. For this reason, although the physical background of the CE phase described above is still not well understood, it has been hypothesized that it plays a crucial role in the formation of a wide variety of binary systems, including double neutron star systems. For a complete review of our current understanding of CE evolution, we refer to the work of Ivanova et al. (2013).

1.2.4 Angular momentum losses

Orbital angular momentum variations, and the mechanisms via which this can occur play an important role in the evolution of a binary since it directly affects the orbital period of the system. Angular momentum can be extracted from a binary system on different timescales (Yakut et al. 2008) mainly via the following processes:

- (i) *Non-conservative mass transfer*: If during mass transfer, the companion star accretes only a fraction of the mass lost from the donor, the rest will carry away some of the specific angular momentum.
- (ii) *Magnetic braking*: As it was mentioned above, the differential rotation of stars is responsible for the production of magnetic fields and, subsequently, magnetized stellar winds. Interactions with the magnetic fields can give rise to tidal effects, causing a rotating star to sync and corotate with the orbit (tidally locked system). If the spin of the star is originally larger than the orbital period, this is essentially translated to angular momentum removal from the binary (see also Rappaport et al. 1983).
- (iii) *Gravitational waves*: These are perturbations of the space-time manifold caused by various kinds of motion and asymmetric distribution of masses in a close binary. Like classical waves, gravitational waves carry energy that is being lost from the system causing the angular momentum to decrease and the orbit to shrink (see also Peters 1964; Riles 2013).

1.2.5 Double neutron star systems

Since the result of this thesis is loosely connected with the possibility of having a double neutron star system, it is appropriate to outline the formation and the importance of these incredible systems. Initially

massive binaries with components close enough to interact with each other, will undergo several stages that are plagued with uncertainties before they end up as neutron stars. The most acceptable scenario for the formation of DNS systems up to this day begins with the evolution of the more massive (primary) component, which naturally evolves on a shorter timescale than its companion. The primary star will fill its Roche-lobe transferring material to the companion star and expose its helium core. Further evolution of the newly formed He-star will lead to a supernova explosion which could unbind the whole system.

If the binary survives the explosion, the first-born neutron star can be detected as a radio pulsar orbiting a massive main sequence star (OB-star). As the latter evolves, mass transfer will be initiated and the system can be observed as a high-mass X-ray binary (HMXB) due to the accelerated infalling material onto the surface of the neutron star. When the secondary star expands to a degree that can engulf the neutron star, a common envelope is formed; assuming that during the spiral-in phase a coalescence of the two stars will not occur, a binary system consisting of a neutron star and a helium star will emerge.

Depending on the mass of the He-star, its evolutionary stage, and the orbital separation of the two components, a second mass transfer event may occur stripping the donor star from its helium-rich envelope and spinning up the accreting neutron star. The neutron star that has been spun up during this process is often dubbed *recycled*.

Finally, the second neutron star will likely be formed in a low-energy supernova (see below). The final fate of such systems, depending on the post-SN orbital separation and eccentricity of the binary, is to merge due to gravitational waves damping. The remnant that is left behind from such an event is most likely a single black hole. All the stages leading to the formation of DNS binaries that were described above are presented in Fig. 1.4 and exhaustively discussed in the work of Tauris et al. (2017).

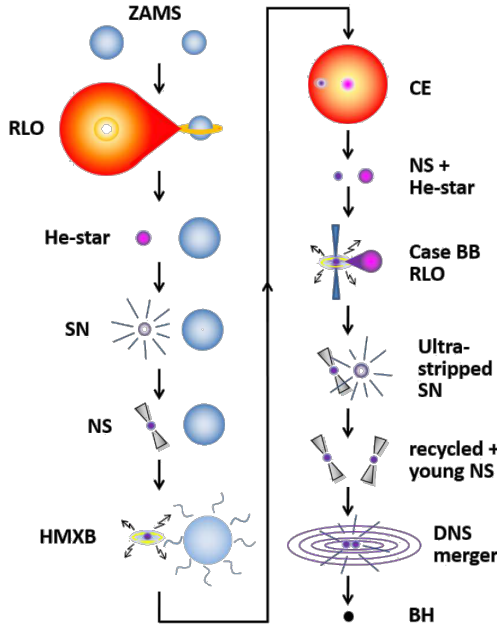


Figure 1.4: Illustration of the overall evolution of a binary system that leads to the formation of a double neutron star system. The resulted binary system merges within a Hubble time and produces a single black hole. Image and caption taken from Tauris et al. (2017).

Double neutron star binaries are remarkable systems and excellent sources of gravitational waves (Abbott et al. 2017). This enables them to act as probes and shed some light on all the uncertain evolutionary stages that lead to their formation, e.g. CE evolution, nature and asymmetries of SNe explosions, velocity kicks imparted onto newborn neutron stars as well as their mass distribution. For a more complete coverage see (Tauris et al. 2017; Ivanova et al. 2003; Dewi & Pols 2003).

1.3 Stellar transients

Transient stars are defined as objects which experience a strong variation in their brightness, that can be observed within a human lifetime, due to various instabilities ranging from magnetic-powered flares in small, dim red dwarfs (M-dwarfs) to thermonuclear shell/core flashes, and gravitational collapse of iron cores. Transients can be non-periodic and/or non-recurring events depending on the nature of the underlying instability. Generally, unstable processes like magnetic reconnection, accretion instabilities, and shell flashes have a tendency not to disrupt the star so they might occur a number of times during the lifetime of the star. On the other hand, known disruptions include supernovae and merging events.

1.3.1 Explosion Mechanisms

Massive stars will end their lives in a supernova (SN) explosion leaving behind a compact object which is either a neutron star or a black hole, depending on the initial mass of the progenitor star, enriching their host galaxy with elements they forged during their lifetime. Classification of supernovae is usually based on their observational characteristics like spectral features, and properties of their light curves as can be seen in the schematic diagram of Fig 1.5 (see [Filippenko 1997](#); [Turatto 2003](#)). In what follows, we will omit the observational characteristics of type-II Supernovae, since they are not directly relevant.

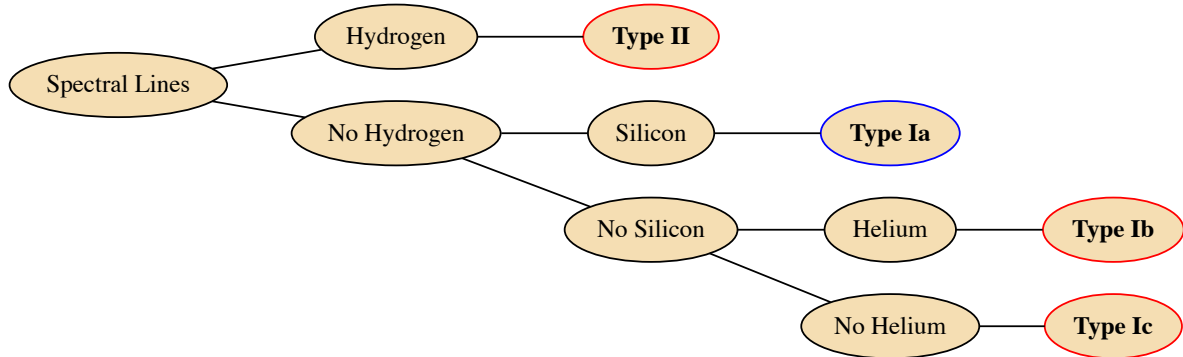


Figure 1.5: Basic classification of supernovae based on spectroscopic features. The absence of hydrogen lines in their spectra, distinguish type I from type II SNe. The presence of silicon, or helium absorption lines, create several subclasses within type I. In any case, further sub-groups can be identified if we take into consideration the behaviour of their light curves.

Whilst there are many physical mechanisms that could potentially lead to a supernova, the connection between the progenitor of the explosion and the type of supernova we eventually observe is still unclear. However, we can differentiate between core collapse SNe (CCSNe) where pressure support is being removed from the core of the star via numerous processes, and thermonuclear explosions of mass-accreting white dwarfs. We will not discuss here the latter case, the associated exploding mechanisms, or how it is related to the type-Ia since it is being mentioned in Section 4.1.1.

For the case of a star that experiences a gravitational core collapse, there are several channels via which pressure support could be removed from the core; next, we discuss a few aspects of these channels and -to a certain degree- the underlying exploding mechanism.

Iron core collapse SNe (Fe-CCSNe)

During the final stages of evolution, if the star is massive enough it will develop an inert iron core. As temperature increases in the core, the energy of the photons becomes sufficiently high to start photodisintegration on the ^{56}Fe nuclei. This process removes pressure from the core, forcing it to contract until electrons and protons fuse together in a process called *neutronization*. As in all weak interactions, neutronization is accompanied by the production of neutrinos that do not contribute to the pressure support against gravity since they escape the star much faster than photons, and effectively acts as a cooling mechanism carrying energy away. Depending on the mass of the core, the degeneracy pressure provided by the neutrons might be sufficient to cease the collapse leading to the formation of a neutron star.

As Müller et al. (2016) mention, the infalling material will bounce on the surface of the neutron star sending back a shock wave that quickly stalls due to photodisintegration of heavy nuclei and neutrino losses; this is the *pre-explosion phase* and it becomes clear that another energy source is needed in order to have a successful explosion. This source is believed to be a (gain) region behind of the shock where energy deposition of neutrinos leads to heating. The shock revival occurs once the accreted material spends sufficient time in the gain region to receive enough energy from neutrinos to negate its binding energy; the shock is re-energized by the radiation and expands outwards again. At this point we have entered the *explosion phase*. In the case of a very massive core, degeneracy pressure from neutrons is not enough to balance the gravitational pressure, therefore the star will continue to collapse forming a stellar mass black hole. More on the progenitors of CCSNe and relevant exploding mechanisms can be found in Smartt (2009); Couch (2017).

Electron capture SNe (ECSNe)

Formation of an iron core is not the only way to remove pressure support. Less massive stars will form a degenerate ONeMg core where the pressure is provided by the degenerate electrons. If the degenerate core reaches a critical mass of $M_{\text{crit}}^{\text{EC}} = 1.37 \text{ M}_\odot$ (Nomoto 1984), electron captures on ^{24}Mg and ^{20}Ne nuclei will reduce the number of electrons, and thus the pressure against gravitational contraction, triggering the collapse of the core. The energy released from the electron captures will eventually lead to an oxygen deflagration⁴. However, since oxygen is ignited in a highly degenerate environment there will be no expansion as a response to the temperature increase, as in the case of non-degenerate matter; instead, this increase of temperature will accelerate the rate of fusion and, consequently, the temperature will again increase in a runaway process. The contraction of the core, due to loss of pressure support, increases the density and leads to more rapid electron captures, at a rate that can overcome the oxygen deflagration and continue to collapse up to neutron star density.

The core is believed to collapse more rapidly than in the case of Fe-CCSNe, launching a shock wave in accordance with core bounce and subsequent neutrino heating as explained above. The final result is a dim supernova with a relatively low explosion energy and low ^{56}Ni ejecta mass (Jones et al. 2016). Two-dimensional simulations have shown that the explosion exhibit almost spherical symmetry (Nomoto et al. 2014) since the rapid nature of the explosion leave less time for asymmetries to develop (Jones et al. 2016), thus ECSNe do not impart large natal velocity kicks to the newly-formed neutron star.

The late evolutionary stages of these lower-mass stars are riddled with uncertainties resulting to a very narrow mass-range for the progenitors of ECSNe. To complicate things even more, if these stars are part of a binary system, interactions between the two stars can give raise to new channels for ECSNe to emerge. For this case, we refer to Siess, L. & Lebreuilly, U. (2018); Giacobbo & Mapelli (2018); Poelarends et al. (2017).

⁴A deflagration process refers to a subsonic front that propagates via thermal conduction as opposed to a detonation process where a supersonic burning front is driven by shock waves.

Pair instability SNe (PISNe)

So far we discussed the final fate of massive stars that develop an iron core, and the less certain evolution of lower-mass stars that develop a degenerate ONeMg core. At the opposite end we find the case of very massive stars, i.e. stars with initial mass $M_{\text{init}} > 100 M_{\odot}$. It has been suggested (Langer 2012) that these enormous stars undergo a dynamical collapse before core oxygen ignition, caused by electron-positron pair creation that effectively reduces the radiation pressure in the stellar core, leaving behind no remnant. PISNe are expected to produce a wide variety of SN types depending on their mass range (Gilmer et al. 2017). We will not discuss further this particular branch of SNe since it poses no interest for this thesis. For this reason, the inquisitive reader is referred to the work of Langer et al. (2007); Woosley (2017); Kozyreva et al. (2017); Gilmer et al. (2017).

1.3.2 Type Ia Supernovae

Supernovae of type Ia play a crucial role in astronomy since they make excellent distance indicators on cosmological scales by acting as standard candles. This is possible due to their characteristic light curves which exhibit a sharp maxima and then gradually fade away. Using techniques such as “time stretching” (Perlmutter 2003) one could bring any type-Ia supernova peak luminosity to a standard candle value. Besides their unique light curves, the spectra of SNe-Ia also appear to be very distinctive with respect to other stellar transients. Typical SNe-Ia spectra lack hydrogen and helium lines, but exhibit a strong silicon line at 615 nm. They are extremely bright events with luminosities that can exceed the value of $10^{10} L_{\odot}$, generated by the radioactive decay of ^{56}Ni that generally its abundance exceeds $0.6 M_{\odot}$.

Although the origins of SNe-Ia is a debatable topic, the generally accepted model involves a carbon-oxygen white dwarf in a binary system that somehow approaches the Chandrasekhar mass limit. This can be achieved mainly via two scenarios; either the WD accretes material from a non-degenerate companion star (known as “single degenerate scenario”), or two WDs spiral-in and merge due to gravitational wave emission (double degenerate scenario). In both cases, a thermonuclear runaway ensues causing the WD to explode. There are several channels within those two scenarios that could initiate an explosive phase, with various observational consequences. For an in-depth discussion, the interested reader can refer also to the work of Hillebrandt & Niemeyer (2000); Wang (2018); Branch & Wheeler (2017).

1.3.3 Type Ib/c Supernovae

Supernova explosions of naked helium stars are expected to be observed as Type Ib or Type Ic due to their lack of a hydrogen mantle (Fig 1.5). Additionally, in order to be classified as Type Ic, the progenitor star must be also stripped from its helium envelope⁵ either via strong stellar winds or binary interactions. As Yoon et al. (2010) mention, population studies indicate that the majority of SNe Ib/c are produced in binary systems without the need of single star progenitors in order to match their observed rate. This can be important since the nature of the explosion will determine if the binary shall remain bound after the explosion or break apart into two loose components.

Of particular interest is the case of *ultra-stripped* SNe as described in Tauris et al. (2015, 2013). The authors showed that a helium star can be heavily stripped as a result of the binary interaction with a neutron star, ultimately leading to a very faint SN-Ic with a mass ejecta of only $\lesssim 0.2 M_{\odot}$. The implication of such small amount of ejecta can be quite important in the formation of DNS systems since the binding energy of the envelopes is expected to be smaller than the one found in normal SNe, imparting only a small kick in the second neutron star.

For an overview of the expected light curve properties of ultra-stripped SNe, see Moriya et al. (2017).

⁵There is a caveat in this formulation; helium can be detected only if it has been excited by the radioactive decay of ^{56}Ni . If a substantial amount of He is present after the explosion but -somehow- shielded from ^{56}Ni , the SN would be still classified (false) as Type Ic! The amount of synthesized ^{56}Ni along with the efficiently mixing into the He-envelope remains crucial for that matter.

1.4 Thesis Outline

In this thesis, we performed numerical calculations with the `MESA` stellar evolution code in order to construct a detailed grid of non-rotating helium stars, and study their viability as supernovae progenitors. The results of our calculations are presented in the following chapters which are organized as follows: in chapter 2, we discuss briefly some basic aspects of the `MESA` stellar evolution code; chapters 3 and 4, are dedicated to the presentation of our simulated results. More specifically, our results are being presented in a series of two papers. In the first one, we suggest a novel progenitor channel for Supernovae-Ia along with a first-order approximation concerning the expected formation rate of the corresponding progenitor systems, energetics of the explosion, and nucleosynthetic signature. In the second one, we further explore the aforementioned progenitor channel of SNe-Ia, by creating a detailed grid of single helium stars in the mass range $0.8 \leq M/M_{\odot} \leq 3.5$ with various initial values of metallicity and overshoot mixing across convective boundaries. Moreover, we elaborate on the importance of residual carbon found in ONe cores, in initiating a thermal runaway leading to the disruption of the star. Finally, chapter 5 summarizes our findings, we discuss the consequences, and suggest future work.

Disclaimer: What follows is an early draft version of the manuscripts submitted for publication to *The Astrophysical Journal Letters*, and to *The Astrophysical Journal*. Differences may appear when compared with the published version. Hence, for citing these papers please refer to the journals.

Chapter 2

METHODS

For the purposes of this thesis we performed numerical calculations using the one dimensional, stellar evolution code **Modules for Experiments in Stellar Astrophysics** (MESA, Paxton et al. 2011; Paxton et al. 2013; Paxton et al. 2015, 2018, 2019). In this section, we briefly discuss the very basic aspects of MESA, and how some key physical concepts are being implemented in the code. The specifics of the input physics we used in our models, are being presented separately in the relevant chapters.

2.1 Modules for Experiments in Stellar Astrophysics

MESA is an open-source stellar evolution code which provides a modular approach to stellar modelling. Each of the available modules is responsible for the delivery of a specific aspect of the required physics (see below) in order to successfully construct a computational stellar model.

For a spherically symmetric star in hydrostatic equilibrium the structure of the star is governed by the following four differential equations, in Lagrangian form

$$\text{Mass conservation: } \frac{\partial r}{\partial m} = \frac{1}{4\pi r^2 \rho} \quad (2.1)$$

$$\text{Hydrostatic equilibrium: } \frac{\partial P}{\partial m} = -\frac{Gm}{4\pi r^4} \quad (2.2)$$

$$\text{Energy conservation: } \frac{\partial l}{\partial m} = \epsilon - \epsilon_\nu + \epsilon_g \quad (2.3)$$

$$\text{Energy transport: } \frac{\partial T}{\partial m} = -\frac{T}{P} \frac{Gm}{4\pi r^4} \nabla = \frac{T}{P} \frac{\partial P}{\partial m} \nabla \quad (2.4)$$

and its evolution by the composition equations (Eq. 2.5)

$$\frac{\partial X_i}{\partial t} = \frac{m_i}{\rho} \left(\sum_j r_{ji} - \sum_k r_{ik} \right), \quad i = 1, \dots, n \quad (2.5)$$

where X_i is the mass fraction of all relevant nuclei $i = 1, \dots, n$ with mass m_i (Kippenhahn et al. 2012, p. 89).

MESA is able to simultaneously solve the coupled structure and composition equations without the need of operator splitting, where we alternately solve the spatial (structure) and temporal (evolution) equations. This is achieved by exploiting a generalized Newton-Raphson iterative solution which is most commonly referred to as the *Heney method* (Wilson 1981; Kippenhahn et al. 2012, p. 106); a grid of finite mesh points has to be set up, essentially dividing the structure into a large number of discrete mass cells where the differential equations need to be calculated. Assuming appropriate boundary conditions, a trial solution has to be guessed in advance which will be later improved after a number of consecutive iterations, and until the required degree of accuracy has been reached in order for the code to converge on a final solution. If after a specified number of iterations the model fails to converge, MESA will retry the calculation using a smaller timestep; this process will be repeated until the code finds an acceptable model to converge or until it reaches a limit in the timestep reduction.

Finally, during the star’s evolution, MESA will automatically adjust the mesh and redistribute it based on the structure and composition profiles of the model at the beginning of each timestep. For a proper insight into timestep selection and mesh refinement see Paxton et al. (2011).

2.1.1 Microphysics

Microphysics modules (e.g. `eos`, `kap`, `rates`, and `net`) provide necessary properties of stellar matter such as equations of state (which relate pressure with density and temperature), opacity tables, and nuclear reaction rates. Here we briefly mention the implementation of the latter, and how we constructed our nuclear reaction network. More information on the specifics of how the microphysics modules are being implemented in MESA can be found in Paxton et al. (2011).

Nuclear networks & reactions rate

The nuclear reaction network that is necessary in order to follow the evolution of a star is provided by either the `net`, or the `jina` module. The former includes basic networks as small as 8 isotopes for modeling the early evolutionary stages of a star, and more extended networks that provide new burning pathways by covering more complicated burning phases, such as hot CNO cycles during novae, and heavy-ion reactions. The `jina` module handles more than 4,500 isotopes, and although it is slower than `net`, it becomes a necessity in cases where large networks cannot be avoided. Both of those modules can be quite flexible since they do not limit the user to work only with the existing networks, but allow for a user-specified nuclear network to be created. This is achieved by providing a list of all desired isotopes and reactions to be considered in the nuclear network, in the form of a data file that is read at run time.

Nuclear burning rates, neutrino loss rates, as well as several other weak reaction rates, are being implemented in MESA via the `rates`, `neu`, and `weaklib` modules. The thermonuclear reaction rates are based on the results of programs such as NACRE (Nuclear Astrophysics Compilation of REaction rates Angulo 1999), which have been calculated in the temperature range from 10^6 K to 10^{10} K, for light nuclei. Weak reaction rates are based on tables or publicly available routines (e.g. Itoh et al. 1996). Nonetheless, these reaction rates are being constantly updated and one should refer to MESA documentation in order to select the optimal set, or provide user-specified reaction rates.

2.1.2 Macrophysics

Utilization of macrophysics modules such as `mlt` and `atm`, allow us to implement various mixing processes (e.g. convection), and apply atmospheric boundary conditions. In this section, we briefly mention how MESA treats mass loss, (semi) convection, and thermohaline mixing. Once again, we refer to Paxton et al. (2011) for a detailed explanation of macrophysics modules implementation.

Mass loss

At each timestep, MESA performs mass adjustments before solving the stellar structure and composition equations since the mass structure of the stellar model has been modified. The mass change can be either due to accretion or losses via winds. Here we discuss only the latter case, which is implemented using several prescriptions that the user specifies (e.g. Glebbeek et al. 2009; de Jager et al. 1988). Nevertheless, one can provide as input constant, or arbitrary rates for the mass-change (\dot{M}) by writing a new `fortran` routine. This routine would calculate \dot{M} for each timestep before calling the Newton-Raphson solver.

The default option in MESA of mass loss rates for massive stars is given by the “Dutch” wind scheme, as described in Glebbeek et al. (2009). Depending on the effective temperature of the star and its surface hydrogen abundance (X), this scheme invokes two different mass-loss rates; for $T_{\text{eff}} < 10,000$ K, it follows the empirical rate from de Jager et al. (1988) in which, the linear approximation of the mass-loss rate is given by

$$\log(-\dot{M}) = 1.769 \log(L/L_{\odot}) - 1.676 \log(T_{\text{eff}}) - 8.158 \quad (2.6)$$

whereas, for $T_{\text{eff}} < 10,000$ K and $X < 0.4$ by mass fraction, it follows the prescription of Nugis & Lamers (2000). In this case, the mass-loss rate has been calculated based on a sample of WN and WC stars, showing a strong dependency on luminosity and chemical composition, and is given by

$$\dot{M} \simeq 1.0 \times 10^{-11} (L/L_{\odot})^{1.29} Y^{1.7} Z^{0.5} \quad (2.7)$$

where \dot{M} is expressed in unit of $M_{\odot}\text{yr}^{-1}$, and Y, Z are the mass fractions of helium and heavier elements respectively.

The mixing length theory

Convection in MESA is treated, by default, as a diffusive process using the standard mixing length theory (MLT) proposed by Cox & Giuli (1968), and is implemented by the `mlt` module. In MLT, a parcel of fluid equipped with some physical properties will rise (or sink) and dissolve in the surrounding environment after it has traveled a characteristic radial distance, called the “*mixing length*, ℓ_{ML} ”. Once the parcel of fluid has been dissolved at a mass coordinate which is different from the one it was originated, it has adopted all the physical properties of the ambient matter, making it indistinguishable from another parcel of fluid located at the same mass coordinate. Commonly, the mixing length is assumed to be of the order of the local pressure scale height¹

$$H_P = \left| \frac{dr}{d \log P} \right| \quad (2.8)$$

whilst MESA gives the option to control the efficiency of convection by specifying an efficiency factor of $\alpha_{\text{ML}} = \ell_{\text{ML}}/H_P$.

As we move towards the surface, the density and temperature decreases which causes convection to be insufficient to carry away the energy flux, and requires a larger temperature gradient. Thus, we define superadiabaticity

$$\delta_{\nabla} \equiv \nabla_T - \nabla_{\text{ad}} \quad (2.9)$$

where ∇_T is the actual temperature gradient, as a measure of the degree to which the actual temperature gradient exceeds the adiabatic value. Hence, in stellar envelopes the energy is being transported mainly by radiation ($\nabla_T \approx \nabla_{\text{rad}}$) despite the fact that convection is still taking place. Computationally, the large

¹As pressure scale height we refer to the radial distance over which the pressure changes by a factor of e (e -folding factor).

superadiabatic gradient can lead to extremely short timesteps in these radiation-dominated convective regions. For this reason, MESA also provides an alternative treatment of convection, known as “MLT++”. Within this framework, the superadiabaticity implied by conventional MLT is being artificially reduced if it exceeds a threshold value that can be specified by the user ($\delta_{\nabla} > \delta_{\nabla, \text{thresh}}$). This allows MESA to calculate models of massive stars up to core collapse. However, as [Paxton et al. \(2013\)](#) mention, the late evolutionary stages of such massive stars can be highly uncertain as these radiation-dominated envelopes may be very unstable, leading to a significant enhancement of mass loss.

Thermohaline & Semiconvection

Semiconvection occurs in regions that are stable to Ledoux criterion but unstable to Schwarzschild

$$\nabla_{\text{ad}} \leq \nabla_{\text{rad}} < \nabla_{\text{ad}} + B \quad (2.10)$$

where B is commonly referred to as the “Ledoux term” of Eq. 1.1 and reads

$$B = -\frac{\phi}{\delta} \nabla_{\mu} \quad (2.11)$$

The Ledoux term accounts for variation of the composition in chemically inhomogeneous regions (i.e. where $\nabla_{\mu} \neq 0$). The gradient of mean molecular weight, μ that characterizes a chemically inhomogeneous region, along with the other terms of Eq. 2.11, are defined as

$$\phi = \left(\frac{\partial \log \rho}{\partial \log \mu} \right)_{P,T}, \quad \delta = - \left(\frac{\partial \log \rho}{\partial \log T} \right)_{P,\mu}, \quad \nabla_{\mu} = \left(\frac{d \log \mu}{d \log P} \right)_s \quad (2.12)$$

The subscripts P , T mean that pressure and temperature are held constant, where the subscript s means the derivative is taken in the surrounding material ([Kippenhahn et al. 2012](#), pp. 49-50).

In MESA, semiconvections is treated as a time-dependent diffusive processes ([Langer et al. 1983](#)), where the diffusion coefficient is calcuted by invoking the `mlt` module

$$D_{\text{SC}} = \alpha_{\text{SC}} \left(\frac{K}{6\rho C_P} \right) \frac{\nabla_T - \nabla_{\text{ad}}}{\nabla_{\text{ad}} + B - \nabla_T} \quad (2.13)$$

where K is the radiative conductivity, C_P is the specific heat at constant pressure, ∇_T is the actual temperature gradient, and α_{SC} is a user-specified, dimensionless efficiency parameter.

Thermohaline mixing is taking place when there is an inversion of the mean molecular weight in regions stable against convection as implied by the Ledoux criterion. MESA treats thermohaline mixing similarly to semiconvection (i.e. as a diffusive process, [Kippenhahn et al. 1980](#)), allowing the user to specify a dimensionless efficiency parameter, α_{TH} according to

$$D_{\text{TH}} = \alpha_{\text{TH}} \frac{3 K}{2\rho C_P} \frac{B}{\nabla_T - \nabla_{\text{ad}}} \quad (2.14)$$

Convective overshooting is also treated by MESA as a time-dependent diffusive process. However we briefly discuss its implementation in Section 4.2.1. For more details on the implementation of the MLT, and other mixing processes we refer to [Paxton et al. \(2011\)](#); [Paxton et al. \(2013\)](#)

Chapter 3

TYPE-IA SUPERNOVAE FROM NON-ACCRETING PROGENITORS

John Antoniadis, Savvas Chanlaridis, Götz Gräfener, and Norbert Langer (2019, in prep)

Abstract

Type Ia supernovae (SNe Ia) are manifestations of helium-deficient stars disrupting in a thermonuclear runaway. While explosions of carbon-oxygen white dwarfs are thought to account for the majority of events, part of the observed diversity may be due to varied progenitor channels. We demonstrate that helium stars with masses between 1.8 and $2.5 M_{\odot}$ may evolve into highly degenerate, near-Chandrasekhar mass cores with helium-deficient envelopes, that subsequently ignite carbon and oxygen explosively at densities $\sim 10^{9.26-9.77} \text{ gr cm}^{-3}$. This happens either due to compression from shell burning (when the core has a hybrid CO/NeO composition), or following ignition of residual carbon triggered by exothermic electron captures on ^{24}Mg (for a NeOMg-dominated composition). We argue that the resulting thermonuclear runaways are likely to prevent core collapse, leading to the complete disruption of the star in a SN Ia explosion with a kinetic energy of $\sim 10^{51} \text{ erg}$. The frequency of progenitor systems would suffice to account for a large fraction of SNe Ia in star-forming galaxies.

Contents

3.1	Introduction	20
3.2	(C)NeO cores: formation and evolution	20
3.2.1	Numerical Calculations: Input Physics	21
3.2.2	Simulation results	22
3.2.3	Late evolution and thermonuclear runaway	23
3.2.4	Energetics and nucleosynthesis	24
3.3	Expected rates and delay times	24
3.4	Summary	27

3.1 Introduction

Despite their central role in Astrophysics and Cosmology, the origin and physics of Type Ia supernovae (SNe Ia) remain uncertain (Maoz et al. 2014). Typical SNe Ia luminosities ($\sim 10^{43} \text{ erg s}^{-1}$) and ejecta velocities ($\sim 10^4 \text{ km s}^{-1}$), require ^{56}Ni masses and kinetic energies of order $\sim 0.6 M_{\odot}$ and $\sim 10^{51} \text{ erg}$ respectively. These properties suggest that SNe Ia are most likely stars that disrupt in thermonuclear explosions, rather than core-collapse events. Carbon/oxygen white dwarfs (CO WDs) approaching the Chandrasekhar-mass limit (M_{Ch}) are the most promising progenitor systems, as they can produce explosions broadly consistent with observations (Nomoto 1982; Churazov et al. 2014).

Conventional stellar evolution channels, produce stable CO WDs with masses below $\sim 1.0 M_{\odot}$. Consequently, matter accretion onto the WD is required to trigger an explosion, either via stable transfer from a donor star (single-degenerate channels; SD), or in a merger event (double-degenerate channels; DD). Thus far, all of the proposed SD or DD variants encounter substantial difficulties in providing a self-consistent model for SNe Ia (Livio & Mazzali 2018). For instance, SD channels require considerable fine-tuning of the mass accretion rate for the WD to grow in mass. In addition, the interaction between the SN blast and the donor star or the circumbinary material, is expected to produce signatures which are rarely or never seen, e.g. some contribution to the SN luminosity at early times (Kasen 2010), radio synchrotron emission (Harris et al. 2016), and H α lines due to unburned hydrogen. DD mergers on the other hand may produce a variety of outcomes, ranging from prompt explosions to long-lived remnants, or the delayed formation of a neutron star (Livio & Mazzali 2018). In addition, their overall contribution to the observed SNe Ia rate may be too low (van Kerkwijk et al. 2010; Claeys et al. 2014; Sato et al. 2015).

Over the past 50 years, systematic studies of SNe Ia explosions have revealed a large diversity in their properties (Taubenberger 2017). Examples of extreme outliers include luminous (e.g. SN 1991T; Filippenko et al. 1992) and ultra-luminous (e.g. SNLS-03D3bb; Howell et al. 2006) SNe, SN 1991bg-like transients which are faint and rapidly evolving (Ruiz-Lapuente et al. 1993), and SN 2012ca-like events, dubbed SNe Ia-CSM, in which there is evidence for interaction with a dense circum-stellar medium (Bochenek et al. 2018). Even among “normal” SNe Ia there is appreciable scatter in rise times, maximum luminosities, ejecta velocities and spectral evolution (Livio & Mazzali 2018). Finally, there seems to be a correlation with environment, as active galaxies typically host more, and brighter SNe Ia (Maoz et al. 2014).

While part of this diversity can be understood within the framework of SD and DD families, there may exist additional evolutionary pathways leading to SNe Ia. Here, we explore an alternative channel in which a thermonuclear runaway leading to a SNe Ia can be initiated during the late evolution of a degenerate core of neon-oxygen (NeO) or carbon-neon-oxygen (CNeO) composition that approaches M_{Ch} . Such progenitors are generally thought to produce massive WDs or electron capture supernovae (ECSN) (e.g., Nomoto & Kondo 1991; Gutierrez et al. 1996; Takahashi et al. 2013). Here however, we show that near- M_{Ch} (C)NeO cores originating from intermediate mass helium stars ($\sim 1.8 - 2.5 M_{\odot}$) —a common product of binary interactions— can ignite their residual carbon and oxygen explosively at densities $\lesssim 10^{9.77} \text{ gr cm}^{-3}$, before the onset of $^{20}\text{Ne}(e^-, \nu_e)^{20}\text{Fe}$ electron capture reactions (Section 3.2). In addition, the envelope is promptly lost via winds or due to binary interactions, leaving behind a helium-free structure. We demonstrate that the combination of final composition and available energy, would yield explosions with luminosities and ejecta velocities consistent with classical SNe Ia (Section 3.2.4). This mechanism does not require accretion from the binary companion and therefore may contribute significantly to the SNe Ia rate in young stellar populations (Section 3.3).

3.2 (C)NeO cores: formation and evolution

Highly degenerate stellar cores of neon-oxygen composition form inside stars with ZAMS masses between 7 and $11 M_{\odot}$ (Farmer et al. 2015; Woosley 2019). After core helium burning, such stars enter a super-asymptotic giant branch (SAGB) phase, characterized by a dense CO core and an extended hydrogen

envelope. As the core becomes increasingly more degenerate, it cools substantially due thermal neutrino emission. An important consequence is that the critical temperature for ^{12}C ignition is first attained off-center, creating a convectively bound flame that propagates inwards (Siess 2006).

Carbon burning in SAGB stars is affected by complex mixing processes due to a combination of inverse composition gradients, overshooting, semi-convection and rotation. The penetration of NeONaMg ashes into unburned regions, may impact significantly the propagation of the burning front. Mixing generally reduces the thermonuclear reaction rate, leaving behind substantial amounts of residual carbon. In extreme cases, the flame can be quenched completely, resulting in a hybrid structure, with a CO core, surrounded by a NeO mantle (Denissenkov et al. 2013).

The subsequent evolution and final fate of the star depend critical on the competition between neutrino cooling due to the presence of $^{23}\text{Na}^{23}\text{Ne}$ and $^{25}\text{Mg}^{25}\text{Na}$ Urca pairs, and compressional heating due to accretion from the helium burning shell (Schwab et al. 2017). SAGB stars are subject to significant dredge-up and thermally unstable shell burning. These effects may impact substantially the ability of the core to grown in mass fast enough.

However, thermal pulses and dredge-up episodes do not occur when the hydrogen envelope is lost, e.g. due to a common envelope (CE) event in a binary system (Woosley 2019). In such a case, helium shell burning is stable, allowing the core to approach the Chandrasekhar mass limit. In what follows, we build detailed numerical models to investigate the combined effects of residual unburned ^{12}C , Urca cooling and constant mass accretion from shell burning, in the late evolution of (C)NeO cores that originate from helium stars.

3.2.1 Numerical Calculations: Input Physics

We use MESA version 10386 to follow the evolution of two helium-star models, M1 and M2, with masses of 2.4 and 1.8 M_\odot respectively. The initial models have uniform compositions with $Y = 0.98$ and $Z = 0.02$ (solar abundances are taken from Grevesse & Sauval 1998). We employ a nuclear network that considers 43 isotopes, from ^1H to ^{58}Ni . Reaction rates are based on the JINA reaclib v2.0 compilation (Cyburt et al. 2010). Electron screening factors and cooling rates from thermal neutrinos are evaluated as in Farmer et al. (2015), and references therein. Weak interaction rates are taken from Suzuki et al. (2016). Wind mass loss rates are calculated using MESA’s Dutch compilation (Paxton et al. 2013).

Our baseline convection model considers standard, thermohaline and semiconvective mixing. Convective stability is evaluated using the Ledoux criterion. By default, MESA uses standard mixing-length theory (MLT; Cox & Giuli 1968) for convective mixing and energy transport. However, following carbon burning, both our models develop dynamically-unstable super-Eddington envelopes, causing numerical difficulties. For this reason, we decided to employ the “enhanced” MLT option available in MESA (Paxton et al. 2013), which artificially reduces the super-adiabatic gradient leading to an enhanced convective energy transport efficiency. This allows us to follow the evolution of the core after carbon burning without interruptions. We further discuss this choice and its impact on the envelope evolution and the final mass in Section 3.4. The MLT mixing length parameter is set to $a_{\text{MLT}} = 2.0$ for both models. For thermohaline and semi-convection we employ the Kippenhahn et al. (1980) and Langer et al. (1983) treatments respectively. In addition to the baseline mixing parameters, in M2, we also consider the effects of overshooting, adopting an efficiency of $f_{\text{ov}} = 0.014$ across all convective boundaries, including the base of the carbon-burning flame. While mixing at this interface may not occur in reality, we use this as a means to quench the flame before reaching the center. Other mixing processes such as rotation and thermohaline can lead to the same outcome for similar initial helium core masses (Farmer et al. 2015). The MESA inlists are publicly available¹. A more extended grid which explores a broad range of initial masses, metallicities and overshooting parameters will be presented in an accompanying paper (Chanlaridis et al. 2019).

¹http://cococubed.asu.edu/mesa_market/inlists.html

3.2.2 Simulation results

Fig. 3.1 shows Kippenhahn diagrams for M1 and M2, focusing on the evolution after central helium depletion. M1 first ignites carbon at mass coordinate $\sim 0.3 M_\odot$, when the total mass is $2.25 M_\odot$ and the

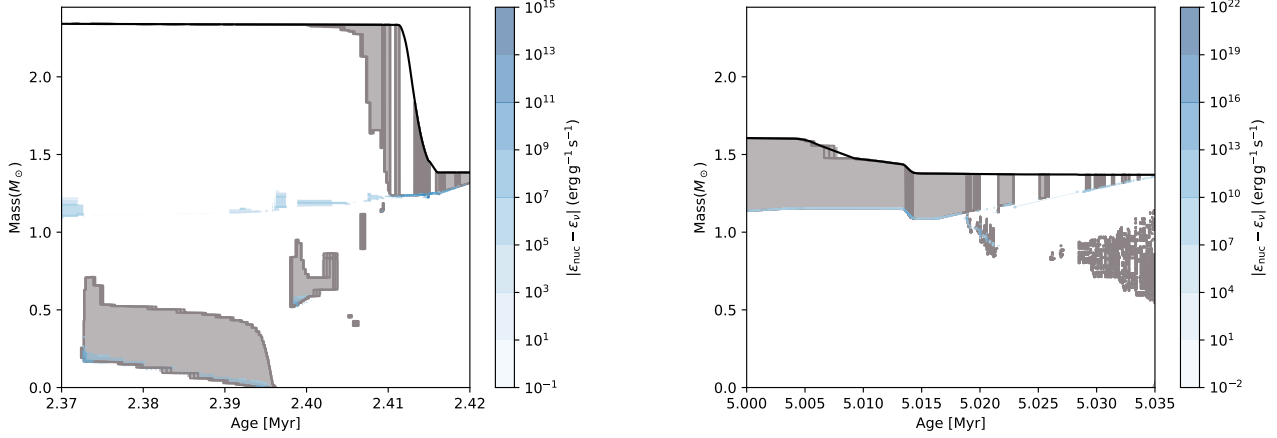


Figure 3.1: Kippenhahn diagrams following the evolution of $M_1 = 2.5 M_\odot$ (left) and $M_2 = 1.8 M_\odot$ He-stars, after core helium depletion. The x-axis represents star's age, whilst the y-axis shows the inner structure of the star in terms of mass coordinate. Colored areas indicate regions in which nuclear burning occurs, i.e. locations for which the nuclear energy ϵ_{nuc} exceeds energy losses due to neutrino emission, ϵ_ν .

CO core has a mass of $\sim 1.15 M_\odot$. The initial flame is followed by secondary flashes which propagate in both directions. Some of these episodes seem to occur only after a small critical mass of carbon has been accumulated below the burning shell. The entire carbon-burning phase lasts for about 40,000 yr. During most of this time, the star is a red giant with a low-density convective envelope ($R \simeq 125 R_\odot$, $\log_{10}(T_{\text{eff}}/\text{K}) \simeq 3.75$, $\log_{10}(L/L_\odot) \simeq 4.3$), and loses mass at a rate of $\dot{M} \simeq 10^{-6} M_\odot \text{ yr}^{-1}$, in good agreement with recent KEPLER models (Woosley 2019).

As the core contracts and its surface gravity increases, the surrounding burning shells become progressively thinner. The envelope responds by expanding and the stellar structure resembles closely that of an SAGB star. The last $\sim 5,000$ yr of the evolution are characterized by rigorous burning in two neighbouring shells which eventually merge, resulting in a ^{20}Ne flash. In this phase the star reaches extremely high luminosities up to $\log L/L_\odot = 6.25$ resulting in a strong stellar wind that lasts for ~ 1000 yr and eventually removes the He-rich envelope.

The evolution of the envelope during the final stages depends critically on the energy transport mechanism above Eddington luminosities. With the enhanced MLT option employed in our calculations, M1 briefly becomes a yellow supergiant as the envelope expands to $R \simeq 900 R_\odot$ while remaining dynamically stable. The strong wind of $\dot{M} \simeq 10^{-3.8} M_\odot \text{ yr}^{-1}$ in this phase is in the same range as theoretically expected maximum values for super-Eddington winds (Owocki et al. 2004; Smith & Owocki 2006).

Conversely, using standard MLT, the envelope becomes dynamically unstable and our calculations encounter numerical difficulties just as the star leaves its Hayashi track, when the core has a mass of $1.32 M_\odot$. By extrapolating the core-growth rate, the star would likely still reach the Chandrasekhar limit (see Woosley 2019, for a similar conclusion). More realistically, binary interactions would easily remove the envelope at this stage, as its binding energy corresponds to only a minuscule fraction of the orbital energy reservoir.

Interestingly, the combination of enhanced mass loss and vigorous burning, leads to the complete depletion of helium in the envelope. Following the thermal flash, the small residual envelope contracts and the wind ceases completely for the last $\sim 5,000$ yr (Fig. 3.1). Our model stops when the star has a

mass of $1.39 M_{\odot}$ (see Sec. 3.2.3).

The surface evolution of M2 is similar (Fig. 3.1). Here, the star expands twice, first for $\sim 5,000$ yr, and then very briefly for some ~ 500 yr, reaching a maximum size of $300 R_{\odot}$. The mass-loss rate however, always remains below $10^{-6} M_{\odot} \text{ yr}^{-1}$. In M2, carbon ignites near mass coordinate $1 M_{\odot}$, just as the star begins to develop an SAGB structure. The flame is quenched after only $0.1 M_{\odot}$ of material has been converted to NeO, leaving behind a hybrid CO/NeO structure. Independently of whether this composition profile survives (Brooks et al. 2017b), the amount of residual carbon is substantial. This model has a final mass of $1.37 M_{\odot}$.

To summarise, during the final evolutionary stages, both models are helium depleted and nearing M_{Ch} . The ability of the core to grow in mass depends somewhat on the uncertain mass-loss rate during the final burning phases. If the envelope is lost too early during the SAGB phase (which does not seem to be the case), then the two stars would leave behind white dwarfs with masses $\leq 1.38 M_{\odot}$, and ONe and CO/ONe composition respectively.

Conversely, if the envelope is retained for long enough, then the central density increases sufficiently to trigger either electron captures on ^{24}Mg or central carbon ignition. In the following section we examine the evolution of the core during this phase.

3.2.3 Late evolution and thermonuclear runaway

Fig. 3.2 gives an overview of the central density and temperature evolution for models M1 and M2.

Following the main carbon-burning episode, both stars continue to contract, while cooling due to neutrino emission. As shell burning intensifies, compressional heating eventually balances off neutrino losses, at $\log_{10}(\rho_c/\text{gr cm}^{-3}) \simeq 8.3$ and 8.0 for M1 and M2 respectively. The subsequent evolution depends on the composition. For M1, the degenerate core is composed mostly of neon and oxygen. The most abundant isotopes have $X(^{16}\text{O}) \simeq 0.43$; $X(^{20}\text{Ne}) \simeq 0.42$; $X(^{24}\text{Mg}) \simeq 0.1$; $X(^{12}\text{C}) \simeq 0.011$; $X(^{23}\text{Na}) \simeq 0.037$; $X(^{25}\text{Mg}) \simeq 0.001$. Between $\log_{10}(\rho_c/\text{gr cm}^{-3}) = 9.05$ and 9.25, the temperature drops to $\log_{10}(T_c/\text{K}) \simeq 8.2$ due to $^{25}\text{Mg}^{25}\text{Na}$ and $^{23}\text{Na}^{23}\text{Na}$ direct Urca reactions. At higher densities, neutrino cooling ceases completely, and the temperature rises again, along the adiabatic curve shown in Fig. 3.2.

When $\log_{10}(\rho_c/\text{gr cm}^{-3}) = 9.65$, exothermic electron captures on ^{24}Mg and ^{24}Na start occurring at a substantial rate, raising the temperature adequately to ignite carbon. In turn, this triggers oxygen burning and a thermonuclear runaway at $\log_{10}(\rho_c/\text{gr cm}^{-3}) = 9.77$. This ignition density is much lower than the $\log_{10}(\rho_c/\text{gr cm}^{-3}) \geq 9.97$ typically expected for oxygen deflagrations in pure NeO cores (Jones et al. 2019). As a consequence, severe deleptonization due to ^{20}Ne electron captures are avoided.

M2 is composed mostly of carbon and oxygen, with $X(^{12}\text{C}) = 0.38$ and $X(^{16}\text{O}) = 0.60$ respectively. Here, ^{23}Na is not abundant enough to cause substantial cooling. Consequently, carbon, which is significantly more abundant compared to M1, ignites at $\log_{10}(\rho_c/\text{gr cm}^{-3}) = 9.26$.

The evolution following central oxygen ignition is not adequately modeled in our 1D simulations. M2 will most likely disrupt in a SN Ia, as the composition and ignition conditions resemble closely those found in standard CO WD progenitors (Nomoto 1982). While the fate of M1 is less certain, a thermonuclear explosion is also the most likely outcome: firstly, the available nuclear energy is sufficient to unbind the star (see below). Secondly, the ignition density is not too much higher than the $\log_{10}(\rho_c/\text{gr cm}^{-3}) \simeq 9.3 - 9.7$ expected for CO WD progenitors. Hence, the deflagration ashes will likely be buoyant, leading to expansion, which will in turn limit the deleptonization rate. This hypothesis is strongly supported by 3D hydrodynamic simulations of ECSN deflagrations by Jones et al. (2019): their least compact progenitor ingites at $\log_{10}(\rho_c/\text{gr cm}^{-3}) = 9.90$ but still manages to eject $\sim 1 M_{\odot}$ of material. Similarly, Marquardt et al. (2015) simulate ONe WD detonations at lower densities and demonstrate that the explosion is practically identical to a typical SN Ia. Interestingly in our 1D simulations, both models experience significant expansion. This is most likely the result of (over-)efficient convection, which also homogenizes the inner $\sim 1 M_{\odot}$ of the core.

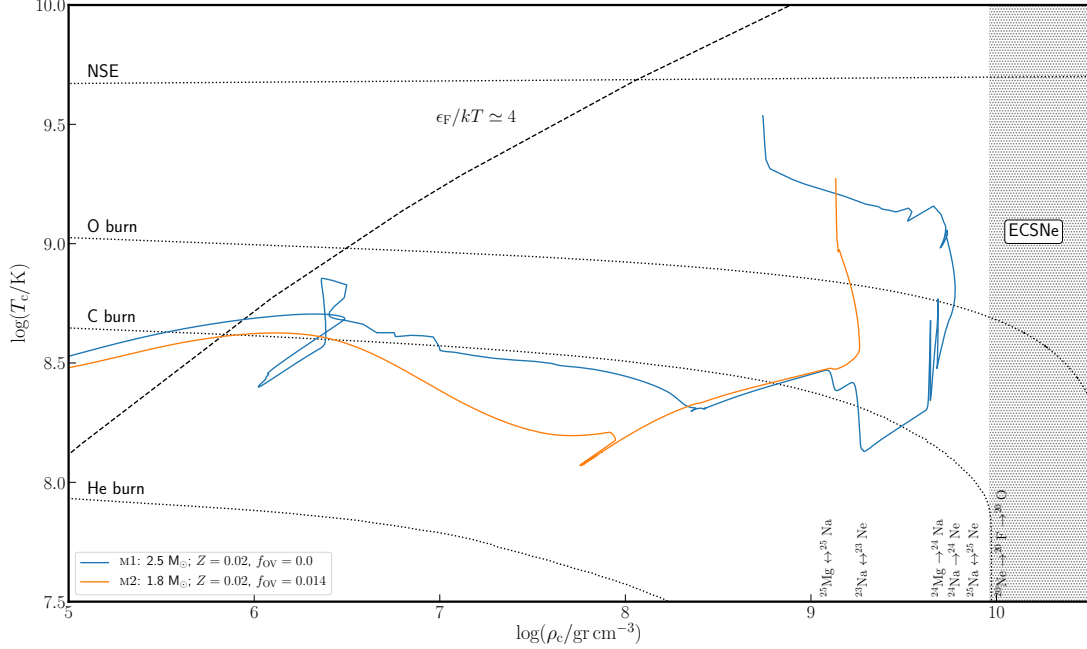


Figure 3.2: Evolution of the core density and temperature for M1 and M2. The dashed line shows the approximate boundary for electron degeneracy. Burning thresholds for a 100% abundance of the corresponding species are indicated with dotted lines. The nuclear statistical equilibrium threshold assumes an equilibrium timescale of 1 s.

3.2.4 Energetics and nucleosynthesis

Fig. 3.3 shows the density profiles of M1 and M2 at maximum compactness, and at the end of our simulations. At the onset of oxygen ignition, M1 and M2 have internal energies (gravitational+thermal) of -5.76 and -5.16 erg, and average electron fractions of $Y_e = 0.496$ and 0.499 for M1 and M2 respectively. If these progenitors were to produce an SNIa of typical composition of $\sim 0.7 M_\odot$ of nickel and iron and $0.6 M_\odot$ of Si-group elements, the corresponding kinetic energies would be $E_{\text{M1}} \simeq 0.83$ and $E_{\text{M2}} \simeq 1.17 \times 10^{51}$ erg, consistent with observations. Obviously, the nucleosynthesis yields depend on the actual Y_e and density profiles during explosive burning. If M1 achieves nuclear statistical equilibrium (NSE) without significant expansion and deleptonization, then it would produce mostly stable iron-peak elements and $\sim 0.3 M_\odot$ of ^{56}Ni , resulting in a sub-luminous explosion. On the other hand, if NSE is achieved after an initial deflagration (Fig. 3.3), then up to $1 M_\odot$ of ^{56}Ni can be produced, with only moderate amounts of iron. Similarly, M2 could produce up to $1.3 M_\odot$ of iron elements if it doesn't expand any further.

3.3 Expected rates and delay times

A useful proxy for the potential (C)NeO/SNIa connection would be a comparison between the Hubble-integrated number of SNeIa, n_{SNIa} , and the expected frequency of stripped near-Chandrasekhar mass (C)NeO cores, n_* . Here, we provide an order-of-magnitude estimate to demonstrate that the two may indeed be similar.

To first order, n_* would be some fraction of the initial star-forming mass that will end up creating (C)NeO cores. Since the envelope needs to be removed before the onset of core helium burning, these

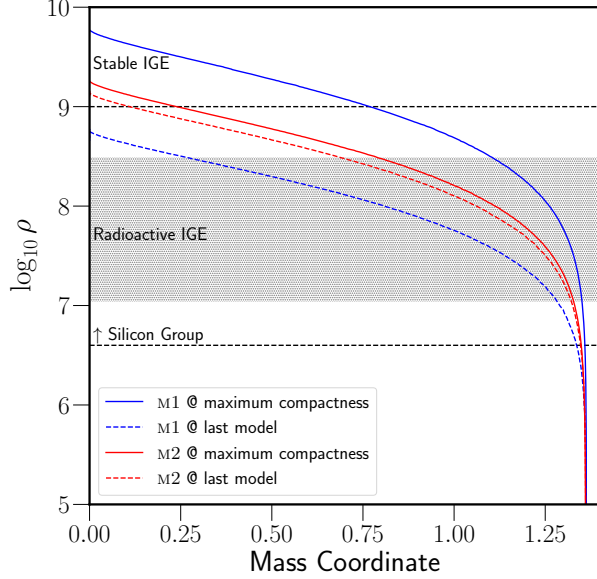


Figure 3.3: Density profiles at maximum compactness (solid lines) and at the end of our MESA calculations (dashed lines). M1 and M2 refer to He-stars with initial mass $2.5 M_\odot$ and $1.8 M_\odot$ respectively. Regions indicating approximate burning regimes as in Seitenzahl & Townsley (2017).

stars would also need to be members of close binary systems, thus:

$$n_* \simeq f_{\text{bin}} \times f_{\text{int}} \times n_{(\text{C})\text{NeO}}. \quad (3.1)$$

Here, $f_{\text{bin}} \simeq 0.7$ (Sana et al. 2012) is the stellar binary fraction, $n_{(\text{C})\text{NeO}}$ is the total number of stars able to form (C)NeO cores, and $f_{\text{int}} \leq 1$ is an efficiency factor to account for the impact of binary interactions (see below).

For binaries, the number of systems with ZAMS masses within a certain range (Fig. 3.4) is:

$$n(m_1, m_2) dm_1 dm_2 = m_1^\alpha q^\kappa dm_1 dq, \quad (3.2)$$

where m_1 is the mass of the primary, here defined as the initially more massive star, $q \equiv m_2/m_1 \leq 1$ is the mass ratio, and a, κ depend on the initial mass function (IMF) and mass-ratio distribution respectively. Integrating, one finds:

$$N = \iint_{m_{\min} q_1}^{m_{\max} q_2} m_1^\alpha q^\kappa dm_1 dq = f \frac{(m_{\min}^{\alpha+1} - m_{\max}^{\alpha+1})(q_1^{\kappa+1} - q_2^{\kappa+1})}{(\alpha + 1)(\kappa + 1)}, \quad (3.3)$$

where f is an appropriate normalization factor. Naively, one would expect the largest contribution from stars that, in isolation, would be able to evolve to the SAGB, viz. stars with ZAMS masses between ~ 7 and $11 M_\odot$ (Farmer et al. 2015). Since accretion is not required to trigger an explosion, *all* primaries and secondaries inside this mass range can potentially contribute to n_* . Hence,

$$(m_{\min}, m_{\max}) = (7, 11) M_\odot; (q_1, q_2) = (0, 1)$$

for the primaries (blue region in Fig. 3.4), and

$$(m_{\min}, m_{\max}) = (11, 125) M_\odot; (q_1, q_2) = (7/11, 1)$$

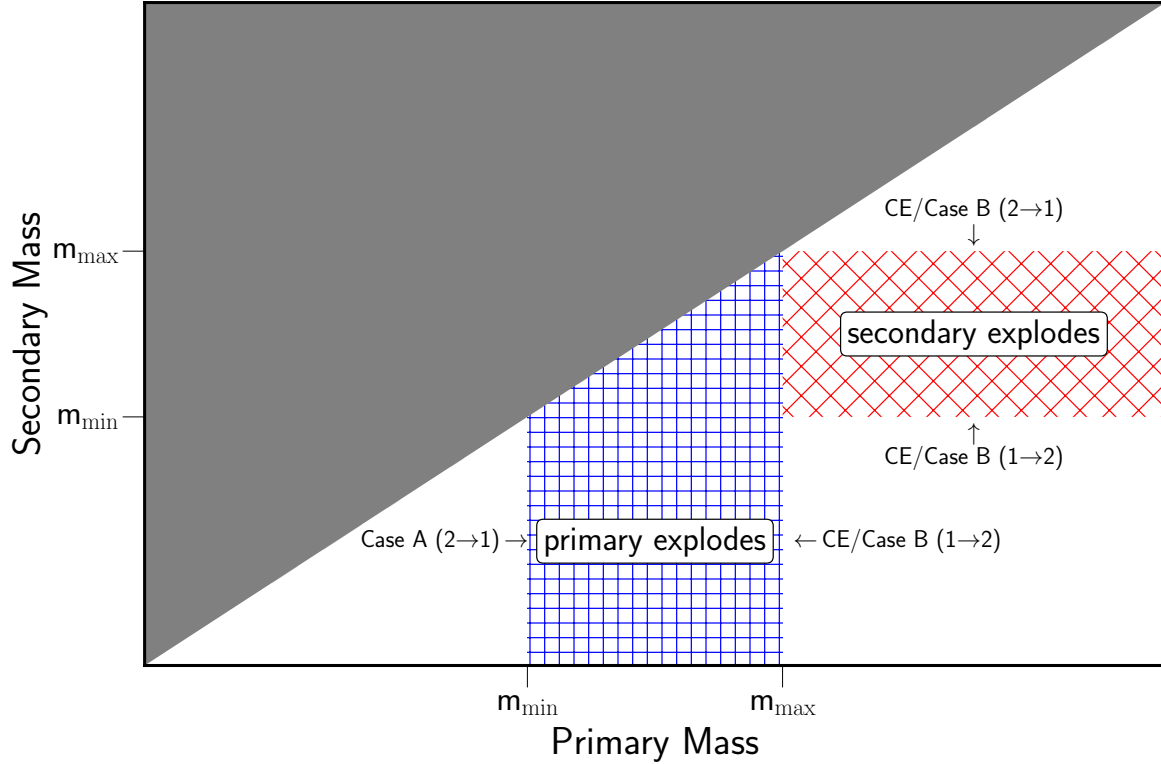


Figure 3.4: Overview of the different systems contributing to the SN Ia channel discussed in the text, on the mass-mass plane. Hatched regions represent initial mass-range for which a thermonuclear explosion may occur. Binary systems outside those mass-ranges can enter the hatched regions via binary interactions, as indicated by the arrows.

for the secondaries (red region). For normalization, we consider all systems within $(m_{\min}, m_{\max}) = (0.1, 125) M_{\odot}$. Adopting a Chabrier (2005) IMF with $a = -2.35$ for $m_1 \geq 1$, and a q -distribution with $k = -0.1$ (Sana et al. 2012), Eq. 3.3 yields, $n_{(\text{C})\text{NeO}} \times f_{\text{bin}} \simeq 5.42 \times 0.7 = 0.0039$ stars per M_{\odot} formed, with the largest contribution ($\sim 80\%$) expected from primaries. For $f_{\text{int}} \simeq 1$, n_{\star} would therefore exceed the number of SN Ia integrated over a Hubble time, $n_{\text{SN Ia}} \simeq 0.002 M_{\odot}^{-1}$ (Maoz et al. 2014).

However, f_{int} is most likely smaller than unity. Firstly, only a fraction of the progenitor binary population will create naked helium stars. Most systems within the hatched regions of Fig. 3.4 will transfer mass to their less massive companions after leaving the main sequence. For the majority of these cases, this process will be dynamically unstable, therefore leading to the removal of the envelope. If this process is indeed efficient, one would expect at least half of the stars to lose their envelopes, hence, conservatively, $f_{\text{int}} \lesssim 0.5$ (Sana et al. 2012).

Following the stripping of the envelope, any subsequent interaction should be sufficiently delayed, for the core to reach M_{Ch} . The post-CE orbital period distribution would generally favor slightly more compact configurations. Hence, only some fraction of the systems will be wide enough to allow a second CE episode after the progenitor has expanded beyond $\sim 100 R_{\odot}$. Nonetheless, a fraction of the closer binaries that will undergo stable case BB Roche-lobe overflow (RLO), could still leave behind stripped (C)NeO cores of sufficiently high mass. For instance, the simulations of Tauris et al. (2015) suggest that a considerable number of helium-free (C)NeO proto-WDs with $m \simeq M_{\text{Ch}}$ can be produced via this channel.

Considering some of the major uncertainties, conservatively, we expect: $0.1 \lesssim f_{\text{int}} \lesssim 0.5$. Taking into account further ambiguities in the IMF and initial configurations, we conclude that $0.05 \lesssim n_{\star}/n_{\text{SNeIa}} \lesssim 1$.

Obviously, the above estimate omits most interactions that could move systems in and out of the hatched regions in Fig. 3.4. Of particular importance may be interactions occurring before the helium-burning phase, as there are roughly three times as many systems with a total mass larger than $7 M_{\odot}$ than there are stars within the hatched regions of Fig. 3.4. A fraction of this population can contribute significantly to the observed rate, after interacting via Case A/B RLO. Additional contributions may come from higher-order multiple systems and/or dynamical interactions in dense environments.

Besides the integrated number of SNeIa, a property that is more challenging to match is the evolution of the SN Ia rate with cosmic time. SNeIa from this channel would have delay times dominated by the main sequence lifetime of the progenitors, i.e. of order 25 to 78 Myr, for stars with ZAMS masses between 7 and $11 M_{\odot}$. Binaries interacting via early Case A RLO prior to the removal of the envelope, could contribute events up to ~ 350 Myr following star formation.

These delay times could help account for the high SN Ia rates in star-forming galaxies (Maoz & Badenes 2010; Claeys et al. 2014). However, some variant of the DD channel would still be required to explain events with much longer delay times.

3.4 Summary

We have shown that stars able to form degenerate (C)NeO cores after losing their hydrogen envelopes, are likely to explode as SNeIa instead of undergoing a core-collapse ECSN. For NeO compositions, the runaway seems to be triggered by the ignition of residual carbon following electron captures on ^{24}Mg , which in turn leads to explosive oxygen burning at densities below $10^{9.77} \text{ gr cm}^{-3}$ (Section 3.2). For hybrid CO/NeO cores, ignition is triggered by core compression, at a density of $10^{9.26} \text{ gr cm}^{-3}$, similar to what is expected for CO WD deflagrations. For either case, the conditions at the onset of oxygen burning are such that the energetics could resemble closely a typical SNeIa (Section 3.2.4). It would be worth considering whether the differences in density and composition could lead to distinct nucleosynthetic signatures that would help distinguish these progenitors and/or contribute uniquely to the chemical evolution of the Galaxy (in analogy to Jones et al. 2019, for ECSNe).

The frequency of the corresponding progenitor systems is sufficient to account for a considerable fraction of the observed SN Ia rate (Section 3.3). Since, the bulk of events would occur only ~ 50 Myr after star formation, this channel is mostly relevant to active late-type galaxies. The shorter delay times compared to traditional SN Ia scenarios, opens further interesting avenues for constraining this model, e.g. with low-metallicity stars.

A similar SN Ia channel has been proposed by Waldman & Barkat (2006) and Waldman et al. (2008), who have also demonstrated that some helium stars with (C)NeO cores can explode before any significant deleptonization occurs. However, these authors do not follow the final evolution stages, and their progenitors still retain a small He-rich envelope at the end. While here we demonstrate that the helium envelope is likely lost only after the core has grown to M_{Ch} , its evolution remains a major uncertainty for this progenitor channel. If helium is removed sufficiently early, e.g. due to binary interactions or dynamical instabilities, then this channel would instead create sub- M_{Ch} (C)NeO WDs. In spite of the mass-loss uncertainties, if viable, this channel would help explain some of the observed SN Ia diversity. Since either star in binary system may potentially explode as a SN Ia without accreting from its companion, the resulting events can resemble setups expected in both SD and DD scenarios. Explosions resulting from the explosion of the secondary, would follow a first core-collapse SN. This could lead to SN Ia remnants with no luminous surviving stars, high proper motions due to a kick from the first SN (like the Kepler remnant, Chiotellis et al. 2012), and possibly associated with a neutron star. Since the envelope can be removed either due to winds, case-BB mass transfer, or a common envelope event, some diversity is also expected in the SN environment. In turn this would influence both the appearance of the

explosion and the evolution of the SN remnant.

Finally this channel seems relevant to other emerging correlations, e.g. the one found between SN locations and the velocity of Si features, or the apparent correlation between SNIa rate and IMF variations at low masses ([Maoz et al. 2014](#)).

Chapter 4

HELIUM STARS AS PROGENITORS OF THERMONUCLEAR SUPERNOVAE

Savvas Chanlارidis, John Antoniadis, G  tz Gr  fener, and Norbert Langer (2019, in prep)

Abstract

In the previous chapter, we have discussed the evolution of two helium stars with initial masses $1.8 M_{\odot}$ and $2.5 M_{\odot}$ that evolve to near-Chandrasekhar (C)ONeMg cores, and subsequently disrupt in a thermonuclear explosion. In this chapter, we further explore this novel SN Ia progenitor channel by performing detailed numerical calculations using MESA in order to investigate the influence of initial metallicity, and overshoot mixing on these degenerate cores. More specifically, we evolved 252 single, non-rotating helium stars in the initial mass range $0.8 - 3.5 M_{\odot}$, covering initial metallicities of $Z = 10^{-4}, 10^{-3}$ and 0.02, and overshoot efficiency factors of $f_{\text{OV}} = 0.0, 0.014$, and 0.016. We find that overshooting during helium burning, between the core and the envelope results in larger cores, thereby prolonging the helium-burning phase. There seems to be a negative correlation between initial metallicity and core growth. We find that carbon ignites off-center for stars with initial masses between $1.3 M_{\odot}$ and $2.8 M_{\odot}$. A subset of these stars with masses between $1.8 M_{\odot}$ and $2.7 M_{\odot}$ evolve into approximately $1.4 M_{\odot}$ (C)ONe cores and likely explode as SN Ia. We also explore the influence of residual carbon during the final evolution of our ONeMg cores by setting the rate of all carbon-participating reactions to zero. We show that under such conditions, these cores will avoid an oxygen ignition at low densities and, most likely, evolve towards an electron capture supernova. Finally, we discuss the influence of envelope ejection mechanisms following the core helium burning phase.

Contents

4.1	Introduction	30
4.1.1	Thermonuclear Supernovae	30
4.1.2	The Urca process	31
4.2	Stellar Evolution Code and Initial Parameter Space	32
4.2.1	Physical assumptions	32
4.3	Results	33
4.3.1	Overview of the Evolution	33
4.3.2	Core Growth and Structure	34
4.3.3	Wind and Envelope Ejection	35
4.3.4	The Role of Residual Carbon	36
4.4	Discussion and Future Work	39

4.1 Introduction

Helium stars (He stars) are the exposed cores of stars that have lost their envelopes due to binary interactions. For progenitor zero-age main sequence (ZAMS) stars in the initial mass range $M_i \approx 7 - 11 M_\odot$ that depends on metallicity and mixing processes (e.g. Ritossa et al. 1996, 1999; Gil-Pons et al. 2005; Siess 2006; Poelarends et al. 2008; Farmer et al. 2015), carbon will be ignited in a shell, following the depletion of helium supply in their cores. Responsible for this off-centre ignition is significant neutrino cooling that occurs deep in the stellar core, and shifts the location of maximum temperature (temperature inversion) to the aforementioned shell. This marks the transition of the star toward the super-asymptotic giant branch (SAGB). The heat generated from the burning shell creates a subsonic carbon-burning front (“C-flame”) that propagates inward. The physical properties of such a deflagration have been the subject of various studies (e.g. Timmes et al. 1994; Siess 2006, 2009; Denissenkov et al. 2013; Farmer et al. 2015) and show a strong dependency on the adopted initial parameters.

As this C-flame moves toward the centre, it will process the material of the partially degenerate carbon-oxygen (CO) core converting it into an oxygen-neon (ONe) core. The subsequent evolution that will determine the final fate of the star, depends on the interplay between the core mass growth rate and the mass loss rate. If shell burning allows the core to reach the critical mass value of $\sim 1.37 M_\odot$ (Nomoto 1984), the central density becomes sufficiently high ($\rho_c \sim 10^{9.95} \text{ gr cm}^{-3}$) for electron captures on ^{24}Mg and ^{20}Ne nuclei to ensue, essentially reducing the pressure in the interior, and ultimately leading to the collapse of the core; this is referred to as *electron capture supernova* (ECSN). The end product of an electron capture induced collapse would be a low-mass neutron star formed from a dim supernova (e.g. Fischer et al. 2010, and references therein) with relatively low explosion energy, which imparts only a small natal kick to the remnant (Knigge et al. 2011; Jones et al. 2013; Jones et al. 2016) compared to the iron core collapse (Fe-CCSN) channel.

On the other hand, if the central density does not reach the threshold for electron captures on the most abundant species, the star will shed its envelope before the core reaches the Chandrasekhar mass limit (M_{ch}), and end up as an ONe white dwarf (ONe WD). However, if the ONe WD is in a close binary system, it can evolve to a supernova following a similar path as the one described above. This can be realized with the transfer of mass from the companion star onto the surface of the WD, allowing it to grow near the Chandrasekhar mass and leave behind a neutron star, a scenario that is known as *accretion-induced collapse* (AIC) (e.g. Nomoto & Kondo 1991; Schwab et al. 2015; Brooks et al. 2017a; Schwab & Rocha 2019).

4.1.1 Thermonuclear Supernovae

Due to lack of a hydrogen envelope, the collapsing core of a He star would be observed as a type Ib/c supernova, depending on the degree of stripping as has been shown by Tauris et al. (2013, 2015). In the case of normal SAGB stars that retain a hydrogen-rich mantle, the spectral lines could resemble the ones found in types IIn-P supernovae (see Moriya et al. 2014, for details).

Nonetheless, one should keep in mind that by the time the effects of electron captures on nuclei cannot be neglected, the necessary pressure gradient against gravity is provided by a strongly degenerate electron gas. For degenerate matter, pressure does not depend on the temperature thus the star can no longer respond to a temperature increase by expanding its outer layers. Since thermonuclear reaction rates are extremely sensitive to temperature variations, under such degenerate conditions, even a small increase of temperature caused by ignition of the existing nuclear fuel, could alter the nuclear burning rate dramatically resulting in a thermal runaway.

Whether the ONe WD undergoes core collapse or experiences a thermonuclear explosion depends on the timescale of electron captures versus the timescale of nuclear energy release. Since electron captures become energetically favorable only above specific values of central density, the ignition location of explosive nuclear burning plays a major role to the final result. Indeed, Jones et al. (2016); Jones et al.

(2019) performed hydrodynamical simulations and were able to demonstrate that for low ignition density, the core does not collapse into a neutron star but rather explodes leaving behind bound remnants.

The consideration above is consistent with the explosion mechanisms (e.g. single degenerate model) related to type Ia supernovae (for recent reviews see Hillebrandt & Niemeyer 2000; Wang & Han 2012; Wang 2018; Livio & Mazzali 2018). It becomes apparent that ECSNe could originate from a variety of progenitor systems either in single or binary configuration, and the connection between the progenitor and the final outcome is far from trivial.

4.1.2 The Urca process

The term “Urca-processes” was introduced by Gamow & Schoenberg (1941) in order to describe energy losses from neutrino emission. It consists of two weak nuclear reactions: an electron capture that operates on a mother nucleus $M \equiv (A, Z)$ forming a more neutron-rich, daughter isobar $D \equiv (A, Z - 1)$



and a beta-decay transition of D back to M



where A and Z denote respectively the mass number and the atomic number of the nucleus. The mother-daughter pair $(_Z^A M, _{Z-1}^A D)$ can be referred to as “Urca nuclei”.

As central density increases, the Fermi energy ϵ_F (or equivalently the electron chemical potential, μ_e) of the relativistic, degenerate Fermi gas prevails over the threshold energy E_t of a given Urca nuclei pair (i.e. the difference between the rest masses of M and D , given by the Q value for a ground-state to ground-state transition), and electron captures will commence promptly. The associated reaction rates (λ^+, λ^-), and neutrino energy losses (L^+, L^-) per nucleon for Eqs. 4.1, 4.2 respectively, have been calculated by Tsuruta & Cameron (1970) and exhibit a strong sensitivity on temperature and density. Therefore, Urca processes become important only for a narrow range of stellar plasma properties, defining a thin Urca shell in which they operate (where $\epsilon_F = E_t$).

Paczynski (1972) argued that during the simmering phase of a CO WD, the energy released from carbon burning would not be able to be transferred efficiently via radiative means leading to a convective core that could engulf the Urca shell (convective Urca). Ultimately, the Urca neutrinos¹ would carry away enough energy to delay the dynamical runaway and forcing the core to move to higher densities thus, collapsing into a neutron star. However, Bruenn (1973) challenged this notion by showing that Urca processes can also have destabilizing effects by generating heat, if convective motions re-position the relevant nuclei at some distance from the Urca shell. In these non-equilibrative states, if e-capture dominates over the β -decay (i.e. if $\rho > \rho_{\text{th}}$), the captured electron creates a “hole” in the Fermi sea and forces another electron to drop from the Fermi surface in order to fill the gap, resulting in heating. On the other hand, if $\rho < \rho_{\text{th}}$, β -decay liberates electrons with excess thermal energy that also results in heating. Therefore, convective Urca processes can either play a major role as local cooling mechanisms (at mass coordinate in the vicinity of the Urca shell where both reactions are in equilibrium) or contribute to heating outside the Urca shell.

The effect of convective Urca processes on stellar interiors remain still an open question and provides up to this day fertile ground for debate. For a more detailed analysis, and fruitful discussion on the physics and importance of Urca process we refer to the work of Paczynski (1973); Barkat & Wheeler (1990); Ritossa et al. (1999); Stein et al. (1999); Lesaffre et al. (2005); Waldman & Barkat (2007); Denissenkov et al. (2015); Schwab et al. (2017).

¹Here we use the term “neutrinos” to refer both to neutrinos and anti-neutrinos interchangeably.

The structure of this paper is organized as follows. In Section 4.2, we present the input physics we used to model the evolution of our He-stars. In Section 4.3, we discuss our results and their implications to our current state of knowledge. Section 4.4 provides a summary of our results and necessary future work.

4.2 Stellar Evolution Code and Initial Parameter Space

We performed numerical calculations using the one dimensional, stellar evolution code Modules for Experiments in Stellar Astrophysics (MESA), version - r10398 (Paxton et al. 2011; Paxton et al. 2013; Paxton et al. 2015, 2018, 2019). Our MESA inlists will become publicly available on http://cococubed.asu.edu/mesa_market/inlists.html.

4.2.1 Physical assumptions

Our grid consists of 252 single He stars in the mass range $0.8 \leq M/M_{\odot} \leq 3.5$ with a step of 0.1. Evolutionary calculations begin with our models being chemically homogeneous. In order to study the effects of metallicity, we create a series of models with low ($Z = 0.0001$), intermediate ($Z = 0.001$), and solar metallicity ($Z \equiv Z_{\odot} = 0.02$), where solar abundances are taken from Grevesse & Sauval (1998). Similarly, for varying the efficiency of overshooting we create series with no overshooting ($f_{ov} = 0.0$), and overshoot mixing ($f_{ov} = 0.014$, $f_{ov} = 0.016$) across all convective boundaries. The free parameter f_{ov} is defined in Herwig (2000) as a fraction of the local pressure scale height, H_p , and is connected to the diffusion coefficient, D_{ov} , via the relation given by Eq. 4.3, where z is the geometric distance from the edge of the convective zone.

$$D_{ov} = D_0 \exp\left(-\frac{2z}{H_v}\right), \quad H_v = f_{ov} \cdot H_p \quad (4.3)$$

The choice of an adequate nuclear network and accurate weak rates are aspects of paramount importance in our considered mass-range, since we expect substantial amounts of ^{23}Na , ^{25}Mg , and ^{27}Al to be produced after the carbon burning phase. Urca process operating on those odd-mass-number nuclei can alter the energy balance with a significant impact upon the thermal structure of the core. For this reason, we construct a nuclear reactions network that consists of forty-three nuclear species, including important NeNa and MgAl cycles, and relevant weak reactions for several Urca pair isotopes. Finally, we incorporate the special weak rates from Suzuki et al. (2016).

We considered ion and electron screening corrections as described in Potekhin et al. (2009) and Itoh et al. (2002) respectively. To account for an enhanced carbon-oxygen mixture as a result of helium burning, we used the Type-2 OPAL Rosseland mean opacity tables (Iglesias & Rogers 1996). For the equation of state blending we followed the options suggested by Schwab et al. (2017).

Convection was treated according to the standard mixing-length theory prescription of Henyey et al. (1965) with a mixing-length parameter of $\alpha_{ML} = 2.0$. Contrary to the standard MLT option provided in MESA, the Henyey et al. (1965) treatment allows the convective efficiency to vary with the opaqueness of the convective element (Paxton et al. 2011). Furthermore, we used the Ledoux criterion for convective instability adopting an efficiency parameter of $\alpha_{SEM} = 1.0$ for semi-convection (Langer 1991), and a diffusion coefficient $D_{TH} = 1.0$ for thermohaline mixing (Brown et al. 2013). Both semi-convection and thermohaline mixing are treated by MESA as diffusive processes (Langer et al. 1983; Kippenhahn et al. 1980).

Mass loss rates due to stellar winds were implemented using the “Dutch” wind scheme (Glebbeek et al. 2009). In our case, this implies two different rates depending on the effective temperature of the star; for $T_{\text{eff}} > 10^4$ K and a surface abundance of hydrogen $X < 0.4$ by mass fraction (which is always satisfied for the models we developed), we apply the prescription of Nugis & Lamers (2000) with a scaling

Table 4.1: Baseline parameters for single helium stars

Parameter	Value(s)
Convection (α_{ML})	2.0
Semiconvection (α_{SC})	1.0
Thermohaline (α_{TH})	1.0
Wind scaling factor (η)	1.0
Overshooting (f_{ov})	0.0, 0.014, 0.016
Metallicity (Z)	10^{-4} , 10^{-3} , 0.02

factor of $\eta = 1$ (canonical value). For $T_{\text{eff}} < 10^4$ K the mass loss rate follows the prescription of de Jager et al. (1988).

4.3 Results

4.3.1 Overview of the Evolution

In a previous paper (Antoniadis et al. 2019, hereafter Paper I), we discussed the expected formation rates, energetics, and nucleosynthetic signature of non-accreting progenitors of SN Ia. In this paper, we follow the evolution of He-stars in the mass range $0.8–3.5 M_{\odot}$ starting with a uniform initial composition. After the end of core helium burning, the newly formed carbon-oxygen core is within the mass range $0.21 \lesssim M_c/M_{\odot} \lesssim 1.86$. The main source of energy moves into a stable, radiative helium-burning shell, whilst the core contracts and cools as a result of neutrino emission. If $M_c \gtrsim 1.1 M_{\odot}$, then the core reaches sufficient high temperature in order to undergo on-centre carbon ignition under non-degenerate conditions, and the star evolves towards an iron core collapse. Otherwise, the core becomes more and more degenerate, allowing us to distinguish the following evolutionary paths.

If the core mass is below a lower limit M_{low} that depends on the adopted values for metallicity and overshooting, then carbon is never ignited and the star will end up as a carbon-oxygen white dwarf.

In the case of $M_{\text{low}} \leq M_c < M_{\text{up}}^{\text{hyb}}$, where $M_{\text{up}}^{\text{hyb}}$ is an arbitrary upper limit that depends on the initial conditions, carbon is ignited off-centre due to a temperature inversion in a similar fashion to typical SAGB stars. The ignition location depends on both the initial mass of the star, and the carbon mass fraction. As long as the temperature at the bottom of the carbon-burning remains higher than the temperature required for carbon ignition, the C-flame advances inward in a series of flashes, but eventually it fails to reach the centre. The flame quenching can be attributed to several physical mechanisms, e.g. overshoot mixing (Denissenkov et al. 2013; Chen et al. 2014; Farmer et al. 2015), and thermohaline mixing (Siess 2009) that mix the processed ONe ashes by dragging them into the CO core, essentially reducing the thermonuclear reaction rate of carbon burning. This results to traces of unburnt carbon that remain in the core (see below), or -in this case- to the complete extinguishment of the flame. In the latter case, the core exhibits a hybrid-like structure, where the inner layers are primarily composed of carbon and oxygen, whilst the outer layers have an oxygen-neon composition. If the star sheds its envelope, the exposed hybrid core will form a hybrid CONe white dwarf, until gravitational settling destroys the stratified structure (see also Brooks et al. 2017b; Schwab & Garaud 2019). Nevertheless, Lecoanet et al. (2016) have shown that buoyancy prevents convective plumes to penetrate into the flame since they are not dense enough, hence convective mixing is insufficient to stall a carbon flame making such hybrid WDs a non-typical product of stellar evolution.

If $M_{\text{up}}^{\text{hyb}} \leq M_c < M_{\text{up}}$, where M_{up} is once again an arbitrary upper limit, the C-flame is able to propagate all the way toward the center, forming an ONe core. However, our simulations show that in all cases, carbon is not being burned up completely, and an amount of $0.0003 \lesssim X(^{12}\text{C}) \lesssim 0.09$ by mass fraction is still present and distributed throughout the inner core. The location of the off-centre

ignition may be key for the amount of unburnt carbon left behind; if the burning is initiated in a layer near the centre, then the burning front reaches the centre on a timescale much shorter than the carbon exhaustion timescale. On the other hand, if the off-centre ignition occurs in a shell rather far away from the centre, the propagation timescale becomes comparable to the carbon depletion timescale (Dominguez et al. 1993).

The presence of carbon may act as a detonator and lead to explosive burning as it has been suggested by (Schwab & Rocha 2019; Waldman & Barkat 2007, hereafter SR19, and WB07 respectively) and Dominguez et al. (1993); García-Berro et al. (1997); Gutiérrez, J. et al. (2005). Moreover, it can heavily influence the ^{56}Ni yields and energetics of the ejecta (Willcox et al. 2016). However, all of these works investigate the effect of residual carbon in a binary system, where carbon is ignited only after a cooled-down WD, has reached the Chandrasekhar limit via accretion (AIC). The ignition density of the runaway may vary with the amount of left-over carbon, resulting in a fairly wide range of ejecta velocities and compositions. In this work, we demonstrate that the Chandrasekhar limit may be achieved via shell burning, without the need of an extended accretion phase. Similar results to our scenario have been obtained by Waldman et al. (2008) for the mass range $2.2 - 2.5\text{M}_\odot$; however, the authors did not follow the evolution past the thin-layer burning stage resulting in the retention of a helium-rich envelope of $\sim 0.1\text{M}_\odot$. The presence of strong He-lines in the observed spectrum could classify the supernova from those progenitors as SN Ia “peculiar”.

4.3.2 Core Growth and Structure

In the next sections, we are going to discuss the growth of hybrid and oxygen-neon cores and how their structure is affected by the metallicity environment and overshoot mixing, without concerning ourselves with the extreme cases of white dwarfs, or core collapsing stellar models.

Following the off-centre carbon burning phase, the core of the star is either dominated by carbon and oxygen which is engulfed in an ONeMg shell, or -if the C-flame reaches the centre- the degenerate core is composed primarily of oxygen and neon, with a small amount of carbon that remains unburnt. In the latter case, we choose a fiducial model of 2.5M_\odot , with solar metallicity and no overshooting, as representative of similar structured models, in order to demonstrate their evolution. The centre contracts and cools down whilst the envelope expands and develops a deep convective region that penetrates into the helium-burning shell as can be seen in Fig. 4.1. The plot shows a cross-section of the helium star in mass coordinates along the y-axis, starting from the center and moving towards the surface of the star, as a function of stellar model number.

The core of our stellar models in the mass range $M_i = 1.8 - 2.7\text{M}_\odot$ grow to near Chandrasekhar masses due to helium shell-burning, and reach a plateau of $M_c \sim 1.36 \pm 0.01\text{M}_\odot$ whilst the extended He-rich envelope is easily ejected via a strong wind (see Section 4.3.3 for discussion). Subsequently, the existing carbon in the core ignites initiating convective motions that feed the core with more carbon, and the star enters a short carbon burning phase. The energy yield from carbon burning is sufficient to raise the temperature for explosive oxygen burning under extreme degenerate conditions to occur. As a result, a thermal runaway ensues and the star which contains no helium at the time of the explosion, it would be observable, most likely, as a SN Ia.

Convective overshooting leads to larger convective cores which, naturally, prolongs the time the star spends in the helium main-sequence phase and thus, lengthens its total lifetime. The reason is that an enlarged convective zone will supply the helium burning core with more fuel. The additional fuel will affect the rate at which nuclear energy is released, thus we expect higher luminosity in the cases where convective overshoot mixing is included. Moreover, the increased size of the metal core will shift the mass range for which we observe the behaviour described above, to lower initial masses. This shifting in the initial mass range caused by the overshoot mixing and the metallicity is more evident and easily understood in Fig. 4.2 where we display the full parameter space in a raster format. The color of each pixel indicates the composition of the star at the time the evolution was terminated. Hatched regions

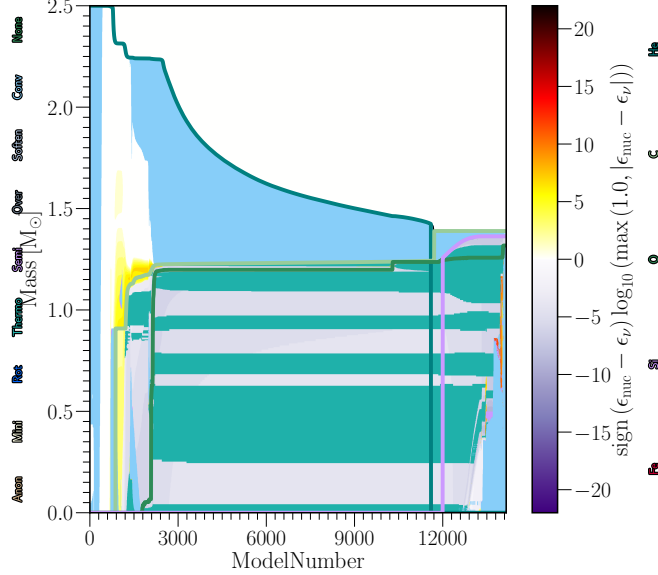


Figure 4.1: Kippenhahn diagram of the $2.5 M_{\odot}$ helium star with $Z = 0.02$ and no overshooting that leads to the final structure shown in Fig. 4.6c. The x-axis is expressed in terms of model number, whilst the y-axis shows the inner structure of the star in terms of mass coordinate. Blue areas denote regions with convection; green-coloured areas indicate thermohaline mixing. The intensity shown in the colour-bar, indicates the net energy-production rate. During electron captures on ^{24}Mg and subsequent carbon burning, the core becomes convective.

represent models that have developed a near-Chandrasekhar mass core whilst, at the same time, most of their envelope has been stripped away. Thus, these are all candidates for undergoing a late thermal runaway, avoiding this was an electron-capture induced implosion. However, we were not able to evolve all of those models up to the point of explosive burning, so we could not accurately constrain the minimum mass fraction of carbon required for such an outcome. It might be the case for some ONe cores in the high end of this mass-range, that the amount of residual carbon is too small to initiate an oxygen deflagration at low densities, and the star will still, most likely, evolve towards an ECSN. Similarly, ONe cores at the lower end of this mass-range could still end up as massive ONe WDs if they don't survive the Urca cooling phase (see below). In this case, the ONe WDs would have a small amount of carbon distributed in their cores.

On the other hand, metallicity seems to adversely affect core growth. The effects of overshooting and metallicity on core growth can be also seen in Fig. 4.3 which shows the final core mass of our stellar models as a function of the initial mass. Missing data points correspond to models for which the code crashed before they were able to get rid of their helium envelope, thus we couldn't follow the evolution past the hot bottom burning phase and obtain a reliable estimate for the final core mass. The scattering that appears at the high-end of our grid is most likely due to the fact that these models stopped at different evolutionary stages; nonetheless, in all of those cases, the core mass has either exceeded the Chandrasekhar mass limit, or the star has developed an ONeSi structure that will eventually lead to a core-collapse, rendering these models irrelevant to our work.

4.3.3 Wind and Envelope Ejection

There are two phases where mass loss through stellar winds can affect the outcome of our model computations. Firstly, because of its long duration, mass-loss in the core helium-burning phase has the potential to reduce the stellar mass, and thus its core size. In our current models the total mass removed in this phase is of the order of $0.1 M_{\odot}$, and its influence on our results is negligible. Secondly, our models reach very high luminosities towards the end of their evolution where the stars are much cooler (up to

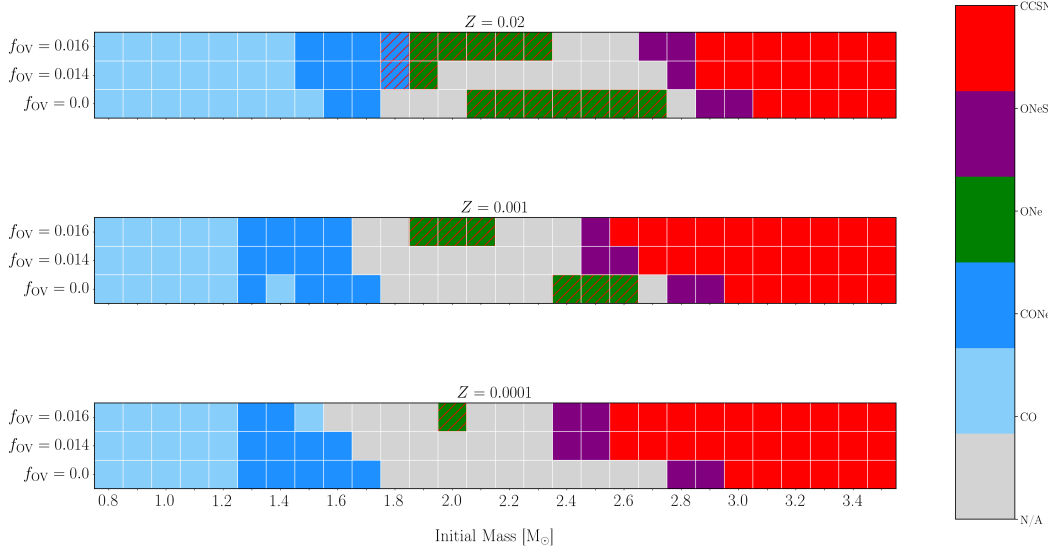


Figure 4.2: Full parameter space of our considered stellar model grid. Metallicity for the bottom, middle, and top panel is $Z = 0.0001$, $Z = 0.001$, and $Z = 0.02$ respectively, whilst the color-bar indicates the composition of the model at the moment our simulation was terminated. Red pixels represent models that have developed a silicon core and will evolve towards a core collapse supernova (CCSN). Hatched regions show models that have developed a core mass in the range $1.35 - 1.37 M_{\odot}$, and can experience a thermonuclear runaway (see text for caveat).

$\log L/L_{\odot} = 6.25$ for the example in Fig. 4.4). In this short phase the remaining He-envelope is removed, which is crucial for the formation of type-Ia SNe in our scenario. For our scenario it is required that that the mass-loss rates in the core He-burning phase are small enough to let the core grow, and that they are high enough in the cool evolved phase to remove the remaining He envelope.

In our models we adopt the “Dutch” MESA wind scheme which extrapolates empirical mass-loss relations for more massive Wolf-Rayet (WR) stars from [Nugis & Lamers \(2000\)](#) for $T_{\text{eff}} > 10^4$ K and uses the prescription of [de Jager et al. \(1988\)](#) for cool stars. These mass-loss rates are very uncertain. Empirically, the mass-loss properties of low-mass He-stars in the range of our models are still very uncertain, mainly because they are only formed in binary systems where they are difficult to observe ([Smith et al. 2017; Zapartas et al. 2017](#)). Recent theoretical works suggest that the mass-loss rates of low-mass helium stars could lie significantly below the relations for massive WR stars ([Gräfener et al. 2017; Vink 2017](#)). This means that the mass-loss rates in the core helium burning phase are most likely small enough to allow our scenario to work.

In late phases, when the degenerate core is near its maximum mass, our models reach extremely high super-Eddington luminosities up to $\log L/L_{\odot} = 6.25$), resulting in a strong stellar wind that eventually removes the He-rich envelope. While the mass-loss rates of cool stars in this regime are also extremely uncertain, it is notable that the maximum values in our models lie in a plausible range near the theoretically expected maximum values for super-Eddington winds ([Owocki et al. 2004; Smith & Owocki 2006](#)).

4.3.4 The Role of Residual Carbon

Oxygen-Neon Cores

As the core is compressed, compressional heating will eventually balance thermal neutrino emission. The core then will continue to compress and heat up until its density reaches the threshold value of various Urca pairs. The $^{25}\text{Mg} - ^{25}\text{Na}$, and $^{23}\text{Na} - ^{23}\text{Ne}$ pairs are of utmost importance in our case, and occur at densities $\log(\rho_c/\text{gr cm}^{-3}) \approx 9.1$, and $\log(\rho_c/\text{gr cm}^{-3}) \approx 9.2$ respectively. [Tsuruta & Cameron \(1970\)](#)

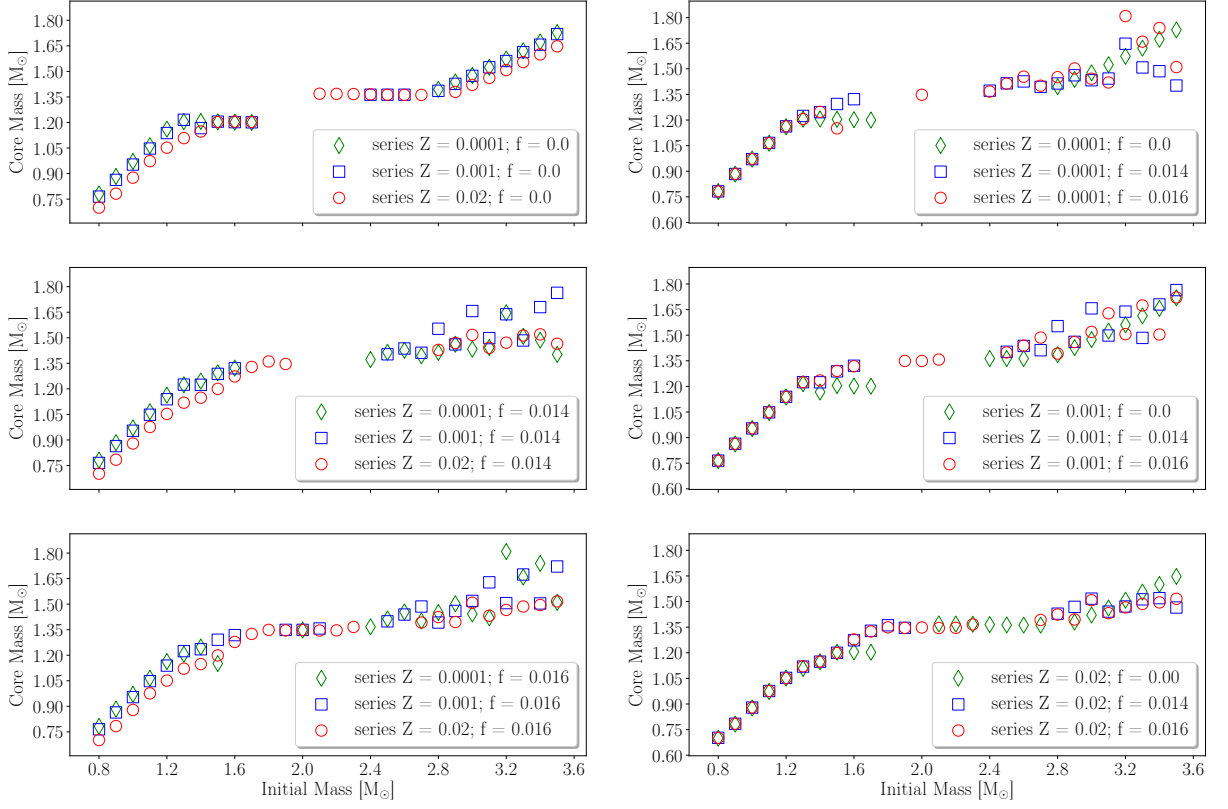


Figure 4.3: Final core mass of our models as a function of initial mass, for various initial metallicities (left) and overshooting factors (right). Models that experience thermal runaway develop a core of $M_c \sim 1.36 \pm 0.01 M_\odot$ (plateau) due to He-shell burning. Missing data points correspond to models which their evolution ended abruptly, hence their final core mass could not be estimated.

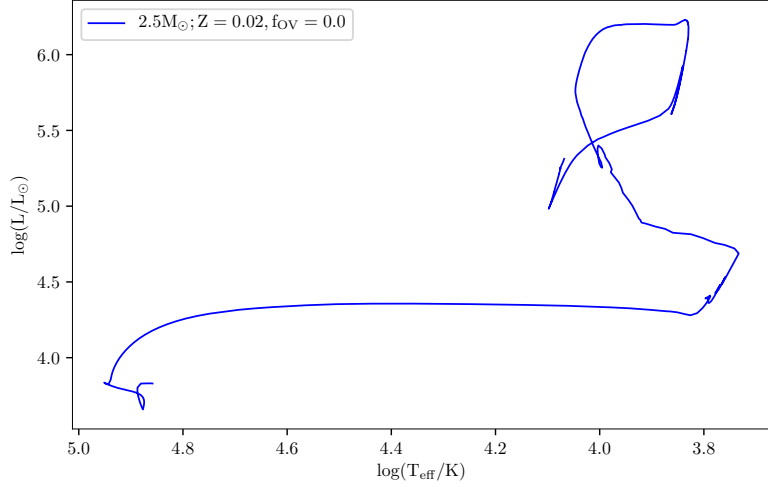


Figure 4.4: Hertzsprung-Russell diagram expressed in terms of luminosity (y-axis) and effective temperature (x-axis), for our $2.5 M_\odot$ fiducial model, starting from helium main sequence phase. During the shell-burning phase, the star reach extremely high, super-Eddington luminosities (up to $\log L/L_\odot = 6.25$) that strips its envelope away.

have shown that the energy loss rate via Urca-cooling depends on the fourth power of temperature ($\propto T^4$), hence this effect is more prominent in our hot, young ONe cores rather than in cooled WDs.

The effect of Urca-cooling can be seen in Fig. 4.5 where the evolution of our fiducial stellar model with initial mass of $2.5 M_{\odot}$, and solar metallicity is being displayed (blue line). The density at which carbon is ignited is illustrated with a dotted black line, taken from MESA; however, MESA assumes a 100% composition of carbon and thus, the limits shown in Fig. 4.5 are only approximated. In our models, Urca-cooling occurs before central density reaches the threshold for carbon ignition, effectively shifting this stage to higher densities by delaying the ignition of carbon, and altering the nucleosynthetic signature of the explosion.

Following the Urca cooling phase, there is no significant neutrino emission and the core evolves along the adiabatic curve of Fig. 4.5. Further compression leads to exothermic e-captures on ^{24}Mg nuclei at $\log(\rho_c/\text{gr cm}^{-3}) \approx 9.6$. The generated heat ignites the residual carbon in a very localized manner due to the sensitivity of carbon reaction rates to temperature. This can be seen as a saw-tooth feature in Fig. 4.5, where heating from carbon burning antagonizes neutrino cooling. We did not investigate the effect of ^{24}Mg mass fraction, however Gutiérrez, J. et al. (2005) have shown that it could play a major role on the subsequent evolution.

The energy yield from carbon burning will eventually lead to dynamical burning of oxygen. Woosley et al. (2004) estimates that the end of the carbon simmering phase occurs roughly at $\log(T_c/\text{K}) \approx 8.9$. In our models, the central temperature at the time the core has reached its maximum compactness is $\log(T_c/\text{K}) \approx 8.82$. Some of these stellar properties are summarized in Table 4.2.

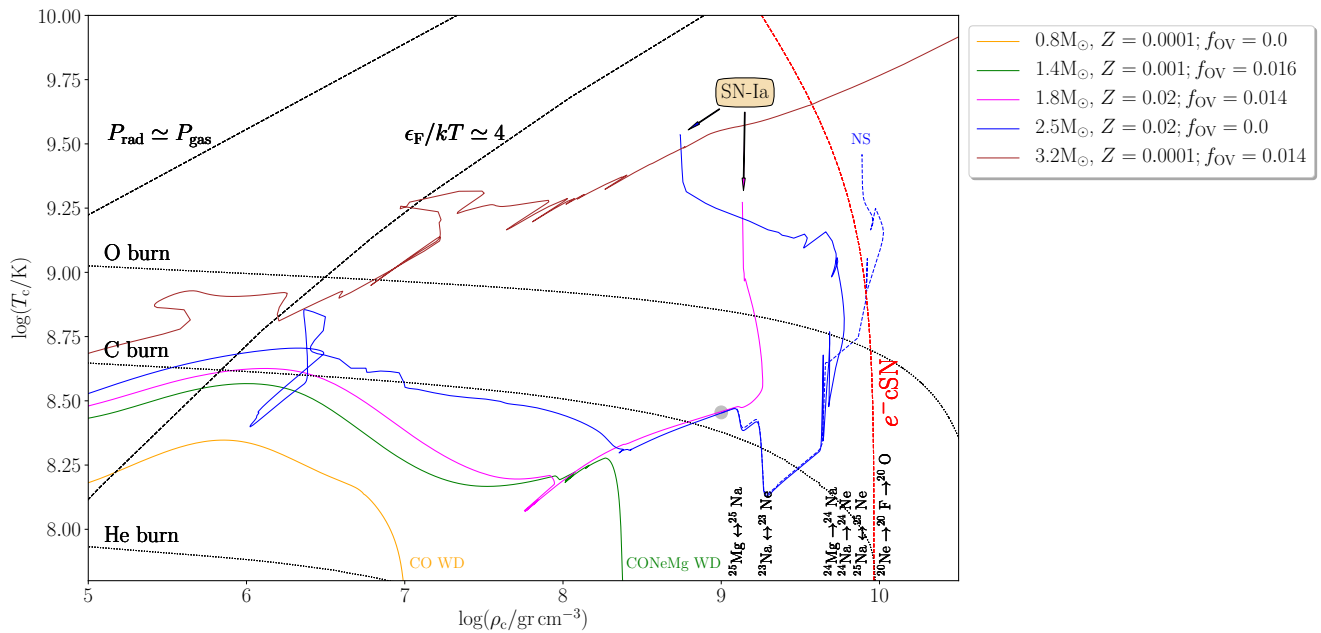


Figure 4.5: Examples of the evolution of different initial masses in the $\log(\rho_c)$ – $\log(T_c)$ plane. Black dotted lines show approximate ignition curves taken from MESA. Black dashed lines indicate different pressure regimes whilst the red dashed curve shows the approximate threshold for e-captures on ^{20}Ne nuclei. The blue dashed line refers to the same stellar model as the one with the solid blue line; the only difference is that for the former, all carbon-participating reaction have been switched off leading most likely to an ECSN.

In order to mimic a carbon-free core and demonstrate the effects of residual carbon, we evolve a series of models for which we have set the rate of all carbon-participating nuclear reactions to zero, once they reached a central density of $\log(\rho_c/\text{gr cm}^{-3}) = 9.0$ for the first time (grey circle in Fig. 4.5). The choice of this density value is quite arbitrary since the cores have a “frozen” carbon profile before the Urca cooling phase. In virtual lack of carbon, the evolution of the core is almost identical to our fiducial model up to the point where electron captures on magnesium occur. From there, compressional heating will once again balance neutrino cooling and the density will continue to grow until it surpasses

the threshold for e-captures on ^{20}Ne nuclei which leads to the ignition of oxygen burning at higher densities. The competition between the propagating oxygen deflagration and e-captures on the post-deflagration nuclear statistical equilibrium (NSE) material will determine the final fate of the star. If the deleptonization of the core due to the electron captures is rapid enough, the core will collapse as a result of pressure support removal. Recently, [Zha et al. \(2019\)](#) found that a deflagration starting from $\log(\rho_c/\text{g cm}^{-3}) > 10.01$ leads to a collapse, reinforcing our notion that a carbon-free ONe core will, most likely, evolve towards an ECSN and ultimately in the formation of a low-mass neutron star. On the other hand, if the oxygen deflagration triumphs over electron captures, [Jones et al. \(2016\)](#) have shown that a thermonuclear explosion will eject a portion of the degenerate core leaving behind an iron-rich, bound remnant.

Hybrid CONeMg Cores

A small number of models develop a CO/ONe structure in their core, but still reach the Chandrasekhar limit. We choose a fiducial model of 1.8M_\odot , with solar metallicity and overshooting ($\text{fov} = 0.014$), in order to demonstrate the evolution of similar structured models. These models ignite carbon and oxygen explosively at even lower densities when compared to the case of non-hybrid stellar models due to the larger mass fraction of carbon they retain.

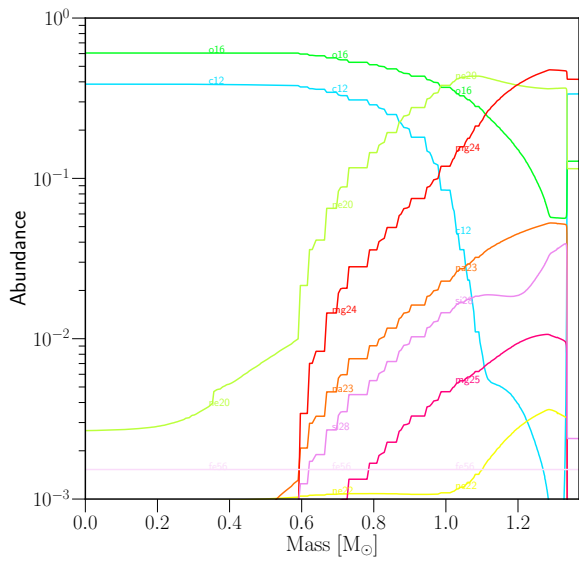
Since the C-flame does not reach the centre, the Urca pairs $^{25}\text{Mg} - ^{25}\text{Na}$, and $^{23}\text{Na} - ^{23}\text{Ne}$, which are byproducts of carbon burning, have not produced in abundance. Thus, Urca cooling does not play any major role in the evolution of hybrid cores. In the absence of the aforementioned Urca pairs, once the timescale of compressional heating is equal to the timescale of thermal neutrino emission, the density will continue to raise until the ignition of carbon, and explosive oxygen burning at lower densities ($\log(\rho_c^{\text{ign}}/\text{gr cm}^{-3}) \approx 9.26$) is initiated. The larger amount of carbon could lead to more energetic explosions (magenta line in Fig. 4.5) compared to the case of ONe cores. The central temperature, when density reaches its maximum value, is $\log(T_c/\text{K}) \approx 8.58$.

The structure of such hybrid proto-WDs is susceptible to mixing due to their composition gradient (see Fig. 4.6a). As [Brooks et al. \(2017b\)](#) mention, the ONe mantle has been processed by a carbon burning front that involves several weak reactions, resulting in a lower electron-to-baryon fraction (Y_e) with respect to the CO core. This configuration is stable against convection as long as the heavier ONe ashes at the top, are much hotter than the lighter CO fuel at the bottom. As the temperature gradient is reduced, the core-mantle interface will be subjected to thermocompositional convection and destroyed in a timescale of the order of Kyr, as the WD moves toward an isothermal profile. By the time an explosion can occur, the WD should be well mixed. The same process can re-distribute the residual carbon within ONe cores and reduce it to such levels so a thermal runaway would be unlikely making the AIC a more plausible scenario.

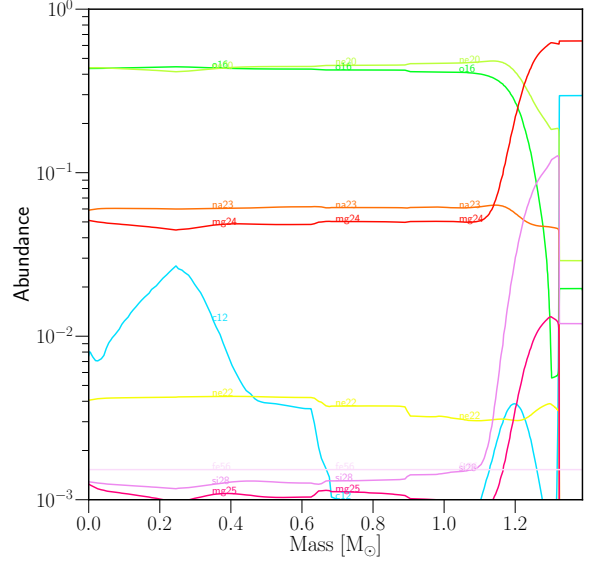
4.4 Discussion and Future Work

In this work, we demonstrated that the evolution of intermediate mass helium stars ($1.8 - 2.7\text{ M}_\odot$) can lead to the formation of near-Chandrasekhar mass (C)ONe cores that ignite oxygen at low central densities, triggered by the burning of left-over carbon, resulting in a thermal runaway and avoiding an electron-capture induced collapse. Helium stars in this mass range are a common product of interacting binary systems, and can lose their helium mantle via winds, case-BB Roche lobe overflow, or in a common envelope event, forming a helium-free structure. Lacking an accretion phase from a donor star, our models may contribute significantly to the observed SN Ia rate (see Paper I for discussion).

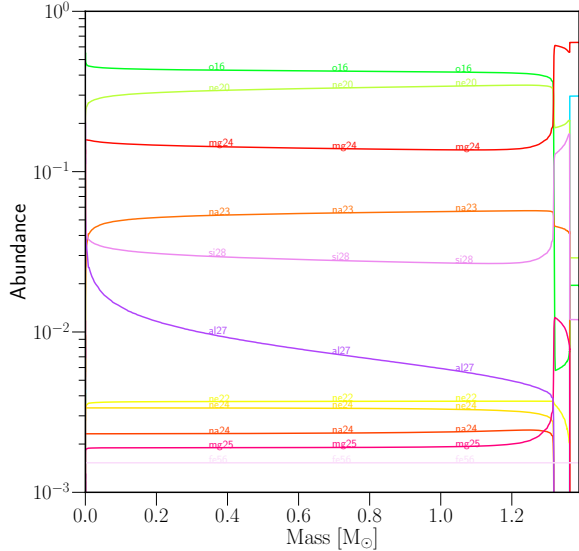
True binary evolution of these cores would help us improve constraints on their progenitor systems, and accurately map mass-loss histories since the binary system may be subjected to early mass transfer episodes leading to effective stripping of the donor star. Moreover, 3D hydrodynamical simulations are required in order to investigate potentially distinct nucleosynthetic yields, and study the energetics of



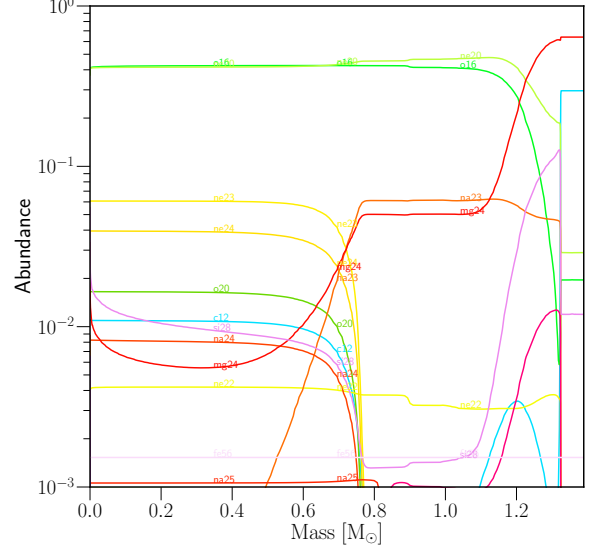
(a) Structure of the $1.8 M_{\odot}$, $Z = 0.02$; $f_{\text{OV}} = 0.014$ stellar model.



(b) Structure of the $2.5 M_{\odot}$, $Z = 0.02$; $f_{\text{OV}} = 0.0$ stellar model. Residual carbon from previous burning stages is visible.



(c) Final structure of the $2.5 M_{\odot}$ stellar model. Residual carbon leads to thermonuclear explosion.



(d) Final structure of the $2.5 M_{\odot}$ stellar model, in the case where carbon consuming nuclear reactions have been turned-off.

Figure 4.6: Abundance profiles of our fiducial models during various evolutionary stages. Panels (a) and (b) refer to the abundance profiles when when $\log(\rho_c/\text{gr cm}^{-3}) \approx 9.0$ (indicated by the grey circle in Fig. 4.5). In panel (d), the core reaches the density threshold for e-captures on Ne nuclei to commence, leading to formation of ^{20}O , and most likely to an ECSN.

Table 4.2: Stellar parameters for twenty-two single helium stars, evolved to the pre-SN stage. Models that were able to evolve after oxygen ignition are indicated with an asterisk in the comments. X_9 refers to the core mass fraction when $\log(\rho_c/\text{gr cm}^{-3}) \approx 9.0$. As ignition density we consider the maximum density before the thermal runaway.

Initial Mass [M_\odot]	Metallicity (Z)	Overshoot (fov)	$X_9(^{12}\text{C})$	$X_{\text{ig}}(^{12}\text{C})$	$X_{\text{ig}}(^{16}\text{O})/X_{\text{ig}}(^{20}\text{Ne})$	$\log(\rho_{\text{c}}^{\text{ig}}/\text{gr cm}^{-3}) = \rho_{\text{c}}^{\text{max}}$	Final core mass [M_\odot]	Comments
1.8	0.02	0.014	0.254	0.25	...	9.26	1.36	Hybrid*
1.8	0.02	0.016	0.136	1.35	Hybrid
1.9	0.001	0.016	0.014	1.35	ONE core
1.9	0.02	0.014	0.061	1.35	ONE core
1.9	0.02	0.016	0.09	1.35	ONE core
2.0	0.0001	0.016	0.0003	1.35	ONE core
2.0	0.001	0.016	0.003	1.35	ONE core
2.0	0.02	0.016	0.05	1.35	ONE core
2.1	0.001	0.016	0.006	1.36	ONE core
2.1	0.02	0.0	0.027	1.37	ONE core
2.1	0.02	0.016	0.01	1.35	ONE core
2.2	0.02	0.0	0.02	1.37	ONE core
2.2	0.02	0.016	0.012	1.35	ONE core
2.3	0.02	0.0	0.011	0.01	0.85	9.75	1.37	ONE core*
2.3	0.02	0.016	0.005	1.37	ONE core
2.4	0.001	0.0	0.006	1.36	ONE core
2.4	0.02	0.0	0.0087	0.0066	0.87	9.75	1.37	ONE core*
2.4	0.001	0.0	0.004	1.36	ONE core
2.5	0.02	0.0	0.0062	0.0057	0.9	9.77	1.36	ONE core*
2.6	0.001	0.0	0.0024	1.36	ONE core
2.6	0.02	0.0	0.0003	1.36	ONE core
2.7	0.02	0.0	0.0027	1.36	ONE core

the explosion. Finally, a more extended parameter space that includes parameters that could alter the evolution of our models (e.g. rotation, wind efficiencies) may prove to be essential (see also Chapter 5).

Chapter 5

CONCLUSIONS AND OUTLOOK

The observed plethora of SNe Ia signatures has created many classification subclasses, which in turn may have originate from distinct channels that have been proposed over the years. Currently, all these channels require a binary system although the explosion mechanism remains annoyingly nebulous.

In this thesis, we suggested a novel Type Ia supernova progenitor channel, that does not require a binary configuration in order to trigger an explosion. Within this paradigm, a low-mass helium star (a natural choice for a SN Ia candidate, since their spectra lack hydrogen lines) develops a degenerate ONe core after an off-centre carbon ignition. Vigorous shell burning allows the core to grow to near-Chandrasekhar mass whilst simultaneously the envelope is ejected via a strong wind. Our models are able to explosively ignite oxygen at low densities during the proto-WD stage, and avoid the core collapse triggered by electron captures. The culprit turns out to be amounts of unburnt carbon that have remained in the core during the earlier propagation of the convectively bound carbon-burning front. Moreover, the carbon flame fails to reach the centre in some of our models creating a hybrid-like structure. Compressional heating may ignite the carbon-rich core in a process that closely resembles typical SNe Ia progenitor channels.

In Chapter 3 we discussed a first-order approximation of the energetics, nucleosynthetic signature, and the expected birth rates of such systems. We found that the available nuclear energy suffices to unbind the star and to produce ejecta with kinetic energies of the order $\sim 10^{51}$ erg, as we would expect from typical SNe Ia. Based on these results we argued that if these systems occur in nature indeed, they can account for a considerable fraction of the observed SNe Ia rate.

In Chapter 4 we performed a more detailed investigation by exploring a stellar model grid of 252 helium stars. Depending on the initial metallicity and overshoot mixing, we constrained the initial mass range of potential candidates to $1.8 - 2.7 M_{\odot}$.

Although 1D stellar evolution modeling consists a great tool, there are several directions that we could take in order to improve upon our models.

- One of the main sources of uncertainty is the accuracy of numerical calculations during the late stages of the evolution. It is unclear if our simulations can accurately reproduce the structure and properties of the outermost layers of stars with convective envelopes. For this reason, more simulations are needed in order to understand the complex underlying physics of stellar winds and envelope ejection.
- In addition, other relevant mechanisms for envelope ejection can arise as a result of several binary interactions. Thus, binary evolution calculations would give us the opportunity to realistically probe various formation channels for our models, and to accurately map the mass-loss history of the binary system. Moreover, such models would enable us to investigate the influence of other parameters such as rotation and magnetic fields.

- The aforementioned binary evolution calculations can provide us with a more accurate parameter space regarding the explosibility of such stars. Based on this parameter space, one could perform population synthesis calculations in order to investigate the arising delay time distribution from such systems, and its connection to our current picture of the delay time distribution of SNIa.
- Advanced 3D hydrodynamical simulations of our progenitor models are required, in order to explore the geometry and the energetics of a potential explosion. Additionally, calculations on time-dependent radiative transfer would give us the opportunity to calculate synthetic spectra and expected light curves from this SNIa channel.
- Accurately predicting nucleosynthetic yields is yet another important aspect that requires 3D modeling. Preliminary results suggest that this channel can give rise to distinct nucleosynthetic signatures that should be traceable in spectra of stars ([Jones et al. 2019](#)).
- Finally, by comparing the aforementioned nucleosynthesis yields with solar and stellar abundances, we can establish stringent observational constraints for this SNIa channel.

BIBLIOGRAPHY

- Abbott, B. P., Abbott, R., Abbott, T. D., et al. 2017, [Phys. Rev. Lett.](#), **119**, 161101
- Angulo, C. 1999, [AIP Conference Proceedings](#), **495**, 365
- Antoniadis, J., Chanlارidis, S., Gräfener, G., & Langer, N. 2019, in prep.
- Barkat, Z., & Wheeler, J. C. 1990, [The Astrophysical Journal](#), **355**, 602
- Bochenek, C. D., Dwarkadas, V. V., Silverman, J. M., et al. 2018, [Monthly Notices of the Royal Astronomical Society](#), **473**, 336
- Branch, D., & Wheeler, J. C. 2017, Supernova Explosions (Springer)
- Brooks, J., Schwab, J., Bildsten, L., Quataert, E., & Paxton, B. 2017a, [The Astrophysical Journal](#), **843**, 151
- . 2017b, [The Astrophysical Journal](#), **834**, L9
- Brown, J. M., Garaud, P., & Stellmach, S. 2013, [The Astrophysical Journal](#), **768**, 34
- Bruenn, S. W. 1973, [The Astrophysical Journal Letters](#), **183**, L125
- Cantiello, M., & Langer, N. 2010, [Astronomy and Astrophysics](#), **521**, A9
- Celletti, A., & Giorgilli, A. 1990, [Celestial Mechanics and Dynamical Astronomy](#), **50**, 31
- Chabrier, G. 2005, [The Initial Mass Function 50 Years Later](#), **327**, 41
- Chanlарidis, S., Antoniadis, J., Gräfener, G., & Langer, N. 2019, in prep.
- Charbonnel, C., & Zahn, J.P. 2007, [Astronomy and Astrophysics](#), **467**, L15
- Chen, M. C., Herwig, F., Denissenkov, P. A., & Paxton, B. 2014, [Monthly Notices of the Royal Astronomical Society](#), **440**, 1274
- Chen, M. C., Herwig, F., Denissenkov, P. A., & Paxton, B. 2014, [Monthly Notices of the Royal Astronomical Society](#), **440**, 1274
- Chiosi, C., & Maeder, A. 1986, [Annual Review of Astronomy and Astrophysics](#), **24**, 329
- Chiotellis, A., Schure, K. M., & Vink, J. 2012, [Astronomy & Astrophysics](#), **537**, A139
- Churazov, E., Sunyaev, R., Isern, J., et al. 2014, [Nature](#), **512**, 406

- Claeys, J. S. W., Pols, O. R., Izzard, R. G., Vink, J., & Verbunt, F. W. M. 2014, *Astronomy & Astrophysics*, **563**, A83
- Clayton, D. 1968, Principles of Stellar Evolution and Nucleosynthesis (McGraw-Hill)
- Couch, S. M. 2017, 375
- Cox, J. P., & Giuli, R. T. 1968, Principles of stellar structure
- Cyburt, R. H., Amthor, A. M., Ferguson, R., et al. 2010, *The Astrophysical Journal Supplement Series*, **189**, 240
- de Jager, C., Nieuwenhuijzen, H., & van der Hucht, K. A. 1988, *Astronomy and Astrophysics Supplement Series*, **72**, 259
- Denissenkov, P. A., Herwig, F., Truran, J. W., & Paxton, B. 2013, *The Astrophysical Journal*, **772**, 37
- Denissenkov, P. A., Truran, J. W., Herwig, F., et al. 2015, *Monthly Notices of the Royal Astronomical Society*, **447**, 2696
- Dewi, J. D. M., & Pols, O. R. 2003, *Monthly Notice of the Royal Astronomical Society*, **344**, 629
- Dominguez, I., Tornambe, A., & Isern, J. 1993, *The Astrophysical Journal*, **419**, 268
- Eggleton, P. 2006, Evolutionary Processes in Binary and Multiple Stars (Cambridge University Press)
- Eggleton, P. P. 1983, *The Astrophysical Journal*, **268**, 368
- Farmer, R., Fields, C. E., & Timmes, F. X. 2015, *The Astrophysical Journal*, **807**, 184
- Filippenko, A. V. 1997, *Annual Review of Astronomy and Astrophysics*, **35**, 309
- Filippenko, A. V., Richmond, M. W., Matheson, T., et al. 1992, *The Astrophysical Journal*, L5
- Fischer, T., Whitehouse, S. C., Mezzacappa, A., Thielemann, F. K., & Liebendörfer, M. 2010, *Astronomy and Astrophysics*, **517**, A80
- Gamow, G., & Schoenberg, M. 1941, *Phys. Rev.*, **59**, 539
- García-Berro, E., Ritossa, C., & Iben, Icko, J. 1997, *The Astrophysical Journal*, **485**, 765
- Giacobbo, N., & Mapelli, M. 2018, *Monthly Notices of the Royal Astronomical Society*, arXiv:1805.11100 [astro-ph.SR]
- Gil-Pons, P., Suda, T., Fujimoto, M. Y., & García-Berro, E. 2005, *Astronomy and Astrophysics*, **433**, 1037
- Gilmer, M. S., Kozyreva, A., Hirschi, R., Fröhlich, C., & Yusof, N. 2017, *The Astrophysical Journal*, **846**, 100
- Glebbeek, E., Gaburov, E., de Mink, S. E., Pols, O. R., & Portegies Zwart, S. F. 2009, *Astronomy and Astrophysics*, **497**, 255
- Gräfener, G., Owocki, S. P., Grassitelli, L., & Langer, N. 2017, *Astronomy and Astrophysics*, **608**, A34
- Grevesse, N., & Sauval, A. J. 1998, *Space Science Reviews*, **85**, 161
- Gutierrez, J., Garcia-Berro, E., Iben, I., et al. 1996, *The Astrophysical Journal*, **459**, 701

- Gutiérrez, J., Canal, R., & García-Berro, E. 2005, *A&A*, 435, 231
- Habets, G. 1986a, *Astronomy and Astrophysics*, 165, 95
- . 1986b, *Astronomy and Astrophysics*, 167, 61
- Hamann, W. R., Koesterke, L., & Wessolowski, U. 1995, *Astronomy and Astrophysics*, 299, 151
- Hamann, W.-R., Schoenberner, D., & Heber, U. 1982, *Astronomy and Astrophysics*, 116, 273
- Han, Z., Podsiadlowski, P., Maxted, P. F. L., & Marsh, T. R. 2003, *Monthly Notices of the Royal Astronomical Society*, 341, 669
- Han, Z., Podsiadlowski, P., Maxted, P. F. L., Marsh, T. R., & Ivanova, N. 2002, *Monthly Notices of the Royal Astronomical Society*, 336, 449
- Harris, C. E., Nugent, P. E., & Kasen, D. N. 2016, *The Astrophysical Journal*, 823, 100
- Heber, U. 2009, *Annual Review of Astronomy and Astrophysics*, 47, 211
- Heger, A., Langer, N., & Woosley, S. E. 2000, *The Astrophysical Journal*, 528, 368
- Heger, A., Woosley, S. E., & Spruit, H. C. 2005, *The Astrophysical Journal*, 626, 350
- Henyey, L., Vardya, M. S., & Bodenheimer, P. 1965, *The Astrophysical Journal*, 142, 841
- Herwig, F. 2000, *Astronomy and Astrophysics*, 360, 952
- Hillebrandt, W., & Niemeyer, J. C. 2000, *Annual Review of Astronomy and Astrophysics*, 38, 191
- Hirschi, R., Meyne, G., & Maeder, A. 2004, *Astronomy and Astrophysics*, 425, 649
- Howell, D. A., Sullivan, M., Nugent, P. E., et al. 2006, *Nature*, 443, 308
- Iben, I. 1997, Scenarios for Type Ia Supernovae, ed. P. Ruiz-Lapuente, R. Canal, & J. Isern (Dordrecht: Springer Netherlands), 111
- Iglesias, C. A., & Rogers, F. J. 1996, *The Astrophysical Journal*, 464, 943
- Itoh, N., Hayashi, H., Nishikawa, A., & Kohyama, Y. 1996, *The Astrophysical Journal Supplement Series*, 102, 411
- Itoh, N., Tomizawa, N., Tamamura, M., Wanajo, S., & Nozawa, S. 2002, *The Astrophysical Journal*, 579, 380
- Ivanova, N. 2015, Binary Evolution: Roche Lobe Overflow and Blue Stragglers, ed. H. M. J. Boffin, G. Carraro, & G. Beccari, 179
- Ivanova, N., Belczynski, K., Kalogera, V., Rasio, F. A., & Taam, R. E. 2003, *The Astrophysical Journal*, 592, 475
- Ivanova, N., & Taam, R. E. 2003, *The Astrophysical Journal*, 599, 516
- Ivanova, N., Justham, S., Chen, X., et al. 2013, *The Astronomy and Astrophysics Review*, 21, 59
- Izzard, R. G., Hall, P. D., Tauris, T. M., & Tout, C. A. 2012, in *IAU Symposium*, Vol. 283, *IAU Symposium*, 95
- Japsen, A.-K., & Klessen, R. S. 2004, *A&A*, 423, 1

- Jones, S., Röpke, F. K., Pakmor, R., et al. 2016, *Astronomy and Astrophysics*, 593, A72
- Jones, S., Hirschi, R., Nomoto, K., et al. 2013, *The Astrophysical Journal*, 772, 150
- Jones, S., Röpke, F. K., Fryer, C., et al. 2019, *Astronomy and Astrophysics*, 622, A74
- Kalogera, V., & Webbink, R. F. 1996, *The Astrophysical Journal*, 458, 301
- Kasen, D. 2010, *The Astrophysical Journal*, 708, 1025
- Kippenhahn, R., Ruschenplatt, G., & Thomas, H.-C. 1980, *Astronomy and Astrophysics*, 91, 175
- Kippenhahn, R., & Weigert, A. 1967, *Zeitschrift für Astrophysik*, 65, 251
- Kippenhahn, R., Weigert, A., & Weiss, A. 2012, *Stellar Structure and Evolution*, 2nd edn. (Springer)
- Klessen, R. S. 2011, in *EAS Publications Series*, Vol. 51, *EAS Publications Series*, ed. C. Charbonnel & T. Montmerle, 133
- Knigge, C., Coe, M. J., & Podsiadlowski, P. 2011, *Nature*, 479, 372
- Kozyreva, A., Gilmer, M., Hirschi, R., et al. 2017, *Monthly Notices of the Royal Astronomical Society*, 464, 2854
- Lamers, H., & Cassinelli, J. 1999, *Introduction to Stellar Winds* (Cambridge University Press)
- Langer, N. 1989, *Astronomy and Astrophysics*, 220, 135
- . 1991, *Astronomy and Astrophysics*, 252, 669
- Langer, N. 2012, *Annual Review of Astronomy and Astrophysics*, 50, 107
- Langer, N., Deutschmann, A., Wellstein, S., & Höflich, P. 2000, *Astronomy & Astrophysics*, 362, 1046
- Langer, N., Fricke, K. J., & Sugimoto, D. 1983, *Astronomy and Astrophysics*, 126, 207
- Langer, N., Heger, A., & Fliegner, J. 1997, in *IAU Symposium*, Vol. 189, *IAU Symposium*, ed. T. R. Bedding, A. J. Booth, & J. Davis, 343
- Langer, N., Norman, C. A., de Koter, A., et al. 2007, *Astronomy and Astrophysics*, 475, L19
- Lauterborn, D. 1970, *Astronomy and Astrophysics*, 7, 150
- Lecoanet, D., Schwab, J., Quataert, E., et al. 2016, *The Astrophysical Journal*, 832, 71
- Lesaffre, P., Podsiadlowski, P., & Tout, C. A. 2005, *Monthly Notices of the Royal Astronomical Society*, 356, 131
- Livio, M., & Mazzali, P. 2018, *Physics Reports*, 736, 1
- Maeder, A. 1987, *Astronomy and Astrophysics*, 178, 159
- Maeder, A., Meynet, G., Hirschi, R., & Ekström, S. 2006, *Rotational Mixing in Massive Stars and Its Many Consequences*, ed. S. Randich & L. Pasquini, 308
- Maoz, D., & Badenes, C. 2010, *Monthly Notices of the Royal Astronomical Society*, 407, 1314
- Maoz, D., Mannucci, F., & Nelemans, G. 2014, *Annual Review of Astronomy and Astrophysics*, 52, 107

- Marquardt, K. S., Sim, S. A., Ruiter, A. J., et al. 2015, *Astronomy and Astrophysics*, 580, A118
- Moriya, T. J., Tominaga, N., Langer, N., et al. 2014, *Astronomy and Astrophysics*, 569, A57
- Moriya, T. J., Mazzali, P. A., Tominaga, N., et al. 2017, *Monthly Notices of the Royal Astronomical Society*, 466, 2085
- Müller, B., Heger, A., Liptai, D., & Cameron, J. B. 2016, *Monthly Notices of the Royal Astronomical Society*, 460, 742
- Nomoto, K. 1982, *The Astrophysical Journal*, 253, 798
- Nomoto, K. 1984, *The Astrophysical Journal*, 277, 791
- . 1987, *The Astrophysical Journal*, 322, 206
- Nomoto, K., Iwamoto, K., & Kishimoto, N. 1997, *Science*, 276, 1378
- Nomoto, K., & Kondo, Y. 1991, *The Astrophysical Journal*, 367, L19
- Nomoto, K., Tominaga, N., & Blinnikov, S. I. 2014, in *American Institute of Physics Conference Series*, Vol. 1594, *American Institute of Physics Conference Series*, ed. S. Jeong, N. Imai, H. Miyatake, & T. Kajino, 258
- Nugis, T., & Lamers, H. J. G. L. M. 2000, *Astronomy and Astrophysics*, 360, 227
- Owocki, S. P., Gayley, K. G., & Shaviv, N. J. 2004, *The Astrophysical Journal*, 616, 525
- Paczyński, B. 1972, *Astrophysical Letters*, 11, 53
- . 1973, *Astrophysical Letters*, 15, 147
- Palacios, A. 2013, in *EAS Publications Series*, Vol. 62, *EAS Publications Series*, ed. P. Hennebelle & C. Charbonnel, 227
- Paxton, B., Bildsten, L., Dotter, A., et al. 2011, *The Astrophysical Journal Supplement Series*, 192, 3
- Paxton, B., Cantiello, M., Arras, P., et al. 2013, *The Astrophysical Journal Supplement Series*, 208, 4
- Paxton, B., Marchant, P., Schwab, J., et al. 2015, *The Astrophysical Journal Supplement Series*, 220, 15
- Paxton, B., Schwab, J., Bauer, E. B., et al. 2018, *The Astrophysical Journal Supplement Series*, 234, 34
- Paxton, B., Smolec, R., Gautschy, A., et al. 2019, arXiv e-prints, arXiv:1903.01426
- Perlmutter, S. 2003, *Physics Today*, 56, 53
- Peters, P. C. 1964, *Phys. Rev.*, 136, B1224
- Podsiadlowski, P. 2014, *The evolution of binary systems*, ed. I. Gonzlez Martnez-Pas, T. Shahbaz, & J. Casares Velzquez, *Canary Islands Winter School of Astrophysics* (Cambridge University Press), 4588
- Poelarends, A. J. T., Herwig, F., Langer, N., & Heger, A. 2008, *The Astrophysical Journal*, 675, 614
- Poelarends, A. J. T., Wurtz, S., Tarka, J., Cole Adams, L., & Hills, S. T. 2017, *The Astrophysical Journal*, 850, 197
- Postnov, K. A., & Yungelson, L. R. 2014, *Living Reviews in Relativity*, 17, 3

- Potekhin, A. Y., Chabrier, G., & Rogers, F. J. 2009, *Phys. Rev. E*, **79**, 016411
- Prialnik, D. 2000, An Introduction to the Theory of Stellar Structure and Evolution (Cambridge University Press)
- Rappaport, S., Verbunt, F., & Joss, P. C. 1983, *The Astrophysical Journal*, **275**, 713
- Riles, K. 2013, *Progress in Particle and Nuclear Physics*, **68**, 1
- Ritossa, C., Garcia-Berro, E., & Iben, Icko, J. 1996, *The Astrophysical Journal*, **460**, 489
- Ritossa, C., García-Berro, E., & Iben, Icko, J. 1999, *The Astrophysical Journal*, **515**, 381
- Roxburgh, I. W. 1998, in Astronomical Society of the Pacific Conference Series, Vol. 138, 1997 Pacific Rim Conference on Stellar Astrophysics, ed. K. L. Chan, K. S. Cheng, & H. P. Singh, 411
- Ruiz-Lapuente, P., Jeffery, D. J., Challis, P. M., et al. 1993, *Nature*, **365**, 728
- Sana, H., de Mink, S. E., de Koter, A., et al. 2012, *Science*, **337**, 444
- Saslaw, W. C., & Schwarzschild, M. 1965, *The Astrophysical Journal*, **142**, 1468
- Sato, Y., Nakasato, N., Tanikawa, A., et al. 2015, *The Astrophysical Journal*, **807**, 105
- Schwab, J., Bildsten, L., & Quataert, E. 2017, *Monthly Notices of the Royal Astronomical Society*, **472**, 3390
- Schwab, J., & Garaud, P. 2019, *The Astrophysical Journal*, **876**, 10
- Schwab, J., Quataert, E., & Bildsten, L. 2015, *Monthly Notices of the Royal Astronomical Society*, **453**, 1910
- Schwab, J., & Rocha, K. A. 2019, *The Astrophysical Journal*, **872**, 131
- Schwarz, R., Bazso, A., Erdi, B., & Funk, B. 2012, *Monthly Notices of the Royal Astronomical Society*, **427**, 397
- Seitenzahl, I. R., & Townsley, D. M. 2017, Nucleosynthesis in Thermonuclear Supernovae, 1955
- Siess, L. 2006, *Astronomy and Astrophysics*, **448**, 717
- Siess, L. 2009, *Astronomy and Astrophysics*, **497**, 463
- Siess, L., & Lebreuilly, U. 2018, *Astronomy and Astrophysics*, **614**, A99
- Smartt, S. J. 2009, *Annual Review of Astronomy and Astrophysics*, **47**, 63
- Smith, N. 2014, *Annual Review of Astronomy and Astrophysics*, **52**, 487
- Smith, N., Gotberg, Y., & de Mink, S. E. 2017, ArXiv e-prints, [arXiv:1704.03516 \[astro-ph.SR\]](https://arxiv.org/abs/1704.03516)
- Smith, N., & Owocki, S. P. 2006, *The Astrophysical Journal Letters*, **645**, L45
- Soberman, G. E., Phinney, E. S., & van den Heuvel, E. P. J. 1997, *Astronomy and Astrophysics*, **327**, 620
- Spruit, H. 2013, *Astronomy and Astrophysics*, **552**, A76
- Spruit, H. C. 2002, *Astronomy and Astrophysics*, **381**, 923

- Stein, J., Barkat, Z., & Wheeler, J. C. 1999, [The Astrophysical Journal](#), 523, 381
- Stothers, R. B., & Chin, C.-W. 1990, [The Astrophysical Journal](#), 348, L21
- Suzuki, T., Toki, H., & Nomoto, K. 2016, [The Astrophysical Journal](#), 817, 163
- Sweigart, A. V. 1997, [The Astrophysical Journal](#), 427, L23
- Szebehely, V. 1967, Theory of Orbits: The Restricted Problem of Three Bodies (Academic Press, New York and London)
- Takahashi, K., Yoshida, T., & Umeda, H. 2013, [The Astrophysical Journal](#), 771, 28
- Taubenberger, S. 2017, [Handbook of Supernovae](#), 317
- Tauris, T. M., Langer, N., Moriya, T. J., et al. 2013, [The Astrophysical Journal Letters](#), 778, L23
- Tauris, T. M., Langer, N., & Podsiadlowski, P. 2015, [Monthly Notices of the Royal Astronomical Society](#), 451, 2123
- Tauris, T. M., & van den Heuvel, E. P. J. 2006, in Compact stellar X-ray sources, ed. W. H. G. Lewin & M. van der Klis, 623
- Tauris, T. M., Kramer, M., Freire, P. C. C., et al. 2017, [The Astrophysical Journal](#), 846, 170
- Timmes, F. X., Woosley, S. E., & Taam, R. E. 1994, [The Astrophysical Journal](#), 420, 348
- Tsuruta, S., & Cameron, A. 1970, [Astrophysics and Space Science](#), 7, 374
- Turatto, M. 2003, in [Lecture Notes in Physics](#), Berlin Springer Verlag, Vol. 598, Supernovae and Gamma-Ray Bursters, ed. K. Weiler, 21
- van der Sluijs, M. V. 2006, PhD thesis, Universiteit Utrecht
- van Kerkwijk, M. H., Chang, P., & Justham, S. 2010, [The Astrophysical Journal](#), 722, L157
- Vink, J. S. 2017, [Astronomy and Astrophysics](#), 607, L8
- Waldman, R., & Barkat, Z. 2006, Ph.D. Thesis
- . 2007, [The Astrophysical Journal](#), 665, 1235
- Waldman, R., Yungelson, L. R., & Barkat, Z. 2008, in Astronomical Society of the Pacific Conference Series, Vol. 391, Hydrogen-Deficient Stars, ed. A. Werner & T. Rauch, 359
- Wang, B. 2018, [Research in Astronomy and Astrophysics](#), 18, 049
- Wang, B., & Han, Z. 2012, [New Astronomy Reviews](#), 56, 122
- Weigert, A. 1968, Mitteilungen der Astronomischen Gesellschaft Hamburg, 25, 19
- Willcox, D. E., Townsley, D. M., Calder, A. C., Denissenkov, P. A., & Herwig, F. 2016, [The Astrophysical Journal](#), 832, 13
- Wilson, R. E. 1981, [Astronomy and Astrophysics](#), 99, 43
- Woosley, S. E. 2017, [The Astrophysical Journal](#), 836, 244
- Woosley, S. E. 2019, [The Astrophysical Journal](#), 878, 49

- Woosley, S. E., Wunsch, S., & Kuhlen, M. 2004, [The Astrophysical Journal](#), 607, 921
- Yakut, K., Kalomeni, B., & Tout, C. A. 2008, ArXiv e-prints, [arXiv:0811.0455](#)
- Yoon, S.-C. 2017, [Monthly Notices of the Royal Astronomical Society](#), 470, 3970
- Yoon, S.-C., & Langer, N. 2005, [Astronomy and Astrophysics](#), 443, 643
- Yoon, S.-C., Woosley, S. E., & Langer, N. 2010, [The Astrophysical Journal](#), 725, 940
- Zapartas, E., de Mink, S. E., Van Dyk, S. D., et al. 2017, [The Astrophysical Journal](#), 842, 125
- Zha, S., Leung, S.-C., Suzuki, T., & Nomoto, K. 2019, arXiv e-prints, [arXiv:1907.04184](#)
- Zingale, M. 2016, equipotentials.py, https://github.com/zingale/astro_animations/blob/master/binary_exoplanets/equipotentials/equipotentials.py